Reexamining the heavy-ion reactions $^{238}U + ^{238}U$ and $^{238}U + ^{248}Cm$ and actinide production close to the barrier

J. V. Kratz,* M. Schädel,† and H. W. Gäggeler‡
Gesellschaft für Schwerionenforschung mbH, 64291 Darmstadt, Germany
(Received 19 July 2013; revised manuscript received 18 October 2013; published 20 November 2013)

Recent theoretical work has renewed interest in radiochemically determined isotope distributions in reactions of ^{238}U projectiles with heavy targets that had previously been published only in parts. These data are being reexamined. The cross sections $\sigma(Z)$ below the uranium target have been determined as a function of incident energy in thick-target bombardments. These are compared to predictions by a diffusion model whereby consistency with the experimental data is found in the energy intervals 7.65–8.30 MeV/u and 6.06–7.50 MeV/u. In the energy interval 6.06–6.49 MeV/u, the experimental data are lower by a factor of 5 compared to the diffusion model prediction indicating a threshold behavior for massive charge and mass transfer close to the barrier. For the intermediate energy interval, the missing mass between the primary fragment masses deduced from the generalized Q_{gg} systematics including neutron pair-breaking corrections and the centroid of the experimental isotope distributions as a function of Z have been used to determine the average excitation energy as a function of Z. From this, the Z dependence of the average total kinetic-energy loss ($\overline{\text{TKEL}}$) has been determined. This is compared to that measured in a thin-target counter experiment at 7.42 MeV/u. For small charge transfers, the values of $\overline{\text{TKEL}}$ of this work are typically about 30 MeV lower than in the thin-target experiment. This difference is decreasing with increasing charge transfer developing into even slightly larger values in the thick-target experiment for the largest charge transfers. This is the expected behavior which is also found in a comparison of the partial cross sections for quasielastic and deep-inelastic reactions in both experiments. The cross sections for surviving heavy actinides, e.g., $_{98}Cf$, $_{99}Es$, and $_{100}Fm$ indicate that these are produced in the low-energy tails of the dissipated energy distributions, however, with a low-energy cutoff at about 35 MeV. Excitation functions show that identical isotope distributions are populated independent of the bombarding energy indicating that the same bins of excitation energy are responsible for the production of these fissile isotopes. A comparison of the survival probabilities of the residues of equal charge and neutron transfers in the reactions of ^{238}U projectiles with either ^{238}U or ^{248}Cm targets is consistent with such a cutoff as evaporation calculations assign the surviving heavy actinides to the $3n$ and/or $4n$ evaporation channels.

DOI: 10.1103/PhysRevC.88.054615 PACS number(s): 25.70.Hi, 25.70.Jj, 25.75.−q, 32.10.Bi

I. INTRODUCTION

The dynamics of heavy-ion low-energy dissipative collisions was recently studied by Zagrebaev *et al.* [1–4] in a model based on multidimensional Langevin equations. This renewed interest in collisions of actinide nuclei was conditioned by the necessity to clarify better than before the dynamics of dissipative collisions in very heavy nuclear systems at low excitation energies and by a search for new ways for production of neutron-rich superheavy nuclei. The mechanism of strongly damped collisions between very heavy nuclei had been studied extensively in the late 1970s in experimental investigations [5–8] of nuclear reactions between two ^{238}U nuclei at energies close to the Coulomb barrier. These were initiated (i) to investigate the gross features of the reaction by measuring product charge, total kinetic energy, and angular distributions [5,6], (ii) to learn about the prospects of synthesizing very heavy actinide isotopes and superheavy elements in their ground states in these damped collisions [7], and (iii) to study fission phenomena of such heavy fragments with atomic numbers up to $Z = 116$ [8]. These early experiments showed that fission of one or both of the colliding nuclei is the dominant process. However, for a given energy dissipation, more particle diffusion was reported [5,6] than previously observed in other collision systems, a feature highly desirable for the syntheses of very heavy elements. In qualitative agreement with this observation, cross sections for surviving heavy actinides were found to exceed those in Ar + U, Kr + U, and Xe + U reactions by typically one order of magnitude [7]. Analyses of the survival probabilities of these highly fissionable nuclei revealed [7] that their formation is associated with the low-energy tails of the excitation-energy distributions. Finally, exclusive investigations of the three-body exit channels using kinematic coincidences with large-area ionization chambers revealed [8] that this reaction channel has to be interpreted as a two-step mechanism with fission following the deep-inelastic collision with minimum scission-to-scission times of 10^{-20} s even for intermediate nuclei with $Z > 110$. However, for the heaviest elements, a considerable broadening of the fission-fragment mass distributions was observed [8]. Similar observations were reported [9] for fusion-fission reactions when the fission barriers approach zero because of high angular momenta. Therefore, the authors of Ref. [8] pointed out that nonequilibrium processes might be involved in the

*Present address: Institut für Kernchemie, Johannes Gutenberg-Universität, 55099 Mainz, Germany; jvkratz@uni-mainz.de
†Present address: Advanced Science Research Center, Japan Atomic Energy Agency, Tokai-mura, Ibaraki 319-1195, Japan.
‡Present address: Paul Scherrer Institut, 5232 Villigen, Switzerland.

sequential fission of the heaviest fragments. Such nonequilibrium processes might occur if these fragments are formed with shape deformations exceeding the deformation of their fission saddle point. It is important to note that these results [8] refer to high values of average total kinetic-energy loss (TKEL) of >150 MeV in the first reaction step, i.e., to a regime of excitation energies that may not be relevant for the production of superheavy elements in their ground states.

These early results on the $^{238}U + ^{238}U$ reaction mechanism had stimulated early theoretical interest [10–15]. Most intimately related to the present work was the theoretical work by Riedel and Nörenberg [13] based on a phenomenological treatment [10–12,14] of dissipative heavy-ion collisions within the diffusion model. The thick-target cross sections of this work at an incident energy of 7.50 MeV/u, reported in a short publication [7], were analyzed with this model [13] to estimate cross sections for the production of superheavy elements as well as probability distributions of excitation energies and spins for the heavy fragments at $\leqslant$7.50 MeV/u. Also, estimates of these probabilities at other incident energies, i.e., 6.49 and 8.30 MeV/u, were given. According to Ref. [13], a higher beam energy improves the chance for the formation of heavier elements even at small excitation energies.

In the present paper, we present a detailed account of the results for the reaction of 7.50 MeV/u ^{238}U ions with thick ^{238}U targets. In addition, we present charge and mass distributions and, in particular, cross sections for surviving heavy actinide isotopes at various other incident energies up to 9.0 MeV/u. These data are used to check our previous conclusions [7] concerning the survival probabilities of the heavy actinide fragments and to compare the energy dependence of the cross sections with diffusion-model predictions [13]. It is shown that large discrepancies between experiment and theory occur at near-barrier energies. Implications of these discrepancies for the prediction of production rates for superheavy elements in $^{238}U + ^{238}U$ collisions are discussed. Consistently with our previous conclusions [7], it is shown that the cross sections for surviving heavy actinides, e.g., $_{98}Cf$, $_{99}Es$, and $_{100}Fm$, indicate that these are produced in the low-energy tails of the dissipated energy distributions. Excitation functions show that identical isotope distributions are populated independent of the bombarding energy, indicating that the same bins of excitation energy are responsible for the production of these fissile isotopes. A comparison of the survival probabilities of the residues of equal charge transfers ΔZ in the reactions of ^{238}U projectiles with ^{238}U and ^{248}Cm targets underlines the previous insight [7] that the surviving heavy actinides are residues of $3n$ and $4n$ evaporation channels.

Motivated by large cross sections for surviving actinides in the $^{238}U + ^{238}U$ reaction and in particular in the $^{238}U + ^{248}Cm$ reaction, bombardments dedicated to the search for superheavy elements were also performed [16,17], however, with negative results.

II. EXPERIMENTAL TECHNIQUES

A. Irradiations

The irradiations were performed at the UNILAC accelerator of the GSI, Darmstadt. The targets were prepared by explosive cladding of 300 and 500 mg/cm^2 thick depleted uranium metal plates onto 1.5-mm-thick copper [18]. The targets were cleaned from a uranium oxide layer by etching with cold concentrated nitric acid prior to irradiation [19] and were then mounted inside a Faraday cup which allowed direct cooling of the backing by deionized water. In two experiments, 3.3 and 3.5 mg/cm^2 thin ^{238}U layers evaporated onto 280 mg/cm^2 Be disks were used. The beam intensity as a function of time and the total charge collected were recorded by a current integrator connected to a multichannel analyzer operated in the multiscaling mode, using time intervals of 30 s. The cup is known to give current readings in 5% agreement with normalizations obtained by Rutherford scattering. The targets were irradiated for 3 hr up to 2 days (beam diameter $\leqslant$10 mm) with beam intensities of 2×10^9 to 2×10^{11} particles/s. The beam energies, effective target thicknesses, and corresponding energy intervals of the various bombardments are listed in Table I. The use of the Northcliffe-Schilling tables [20] for the calculation of effective target thicknesses is justified by results of energy-loss measurements [21] for ^{238}U energies between

TABLE I. Summary of bombardments of metallic ^{238}U targets with ^{238}U and ^{136}Xe ions.

Projectile	Length of bombardment (d)	Integral particle number (particles)	Incident laboratory energy E_i (MeV/u)	E_i/B[a]	Effective target thickness (atoms/cm^2)	Exit laboratory energy E_{ex} (MeV/u)
^{238}U	1.83	1.62×10^{16}	6.49	1.07	4.21×10^{18}[b]	6.06
	0.69	1.14×10^{16}	6.84	1.13	9.06×10^{18}[b]	6.06
	0.13	3.04×10^{13}	7.50	1.24	1.75×10^{19}[b]	6.06
	0.19	3.12×10^{14}	7.50	1.24	1.75×10^{19}[b]	6.06
	1.23	7.29×10^{15}	7.50	1.24	1.75×10^{19}[b]	6.06
	2.23	4.90×10^{15}	8.65	1.43	3.23×10^{19}[b]	6.06
	0.63	5.13×10^{15}	8.30	1.37	8.35×10^{18}	7.65
	1.94	1.43×10^{16}	9.00	1.48	8.85×10^{18}	8.31
^{136}Xe	1.00	1.11×10^{17}	7.50	1.40	3.4×10^{19}[b]	5.95

[a]Incident energy E_i relative to the laboratory barrier B, calculated with an interaction radius $R = 16.89$ fm [6] for the $^{238}U + ^{238}U$ reaction and $R = 15.47$ fm for the $^{136}Xe + ^{238}U$ reaction.

[b]Infinitely thick target. The effective target thickness is defined by the calculated range [20,21] of the projectile in metallic ^{238}U between the incident energy E_i and the exit energy $E_{ex} = B$.

5.9 and 10 MeV/u, which were found to be in agreement with the tabulated values. Owing to the reaction kinematics, all reaction products were stopped in the target itself or in the Be substrate of the target.

Experiments with ^{248}Cm targets were performed with 10 MeV/u ^{238}U ions. Metal targets containing 3.2 and 7.27 mg/cm^2 ^{248}Cm (97% isotopic purity) were produced by evaporation onto Mo foils [22]. Before the beam entered the ^{248}Cm targets, windows and cooling gas reduced the energy to 7.40 MeV/u as ascertained by measurements with a surface-barrier detector. The target thicknesses were sufficient to degrade the beam energy E further to near or below the Coulomb barrier B ($1.18 \geqslant E/B \geqslant 1.09$ or 0.96). Reaction products emitted within laboratory angles $\leqslant 55^\circ$ were stopped in a copper catcher that was subsequently subject to chemical separations.

B. Chemical separations

After the end of irradiation, the target was removed from the Faraday cup and connected with a closed glass apparatus allowing dissolution of the active target and substrate area and performance of distillation during and after the dissolution process. Complete dissolution of all produced radioactivities was checked by x-ray spectroscopy. For the measurement of charge and mass distributions, the reaction products were separated into up to 25 chemical fractions containing elements and element groups with Z ranging from 26 to 100 using a modified separation scheme based on the method of Kratz *et al.* [23]. Separate experiments involving mainly the chemical separation of individual actinides [19] were also performed. In the ^{248}Cm bombardments, the copper catchers served to separate chemical fractions of Po, At, Cm through No, by gas-phase or high-performance liquid chromatography [19]. Chemical yields were determined gravimetrically or via long-lived radioactive tracers of the same element added to the system prior to dissolution or by following radioisotopes of elements with a similar chemical behavior, which could be identified among the nuclear reaction products by nuclear spectroscopy. The determination of chemical yields for the actinide elements was based on measured chemical yields of homologous lanthanide elements. Commercially available actinide tracers were not used for the chemical-yield measurements because the same isotopes are formed in the nuclear reaction. Details are given elsewhere [19]. The fractions were prepared as counting samples by precipitation and filtration, by evaporation on tantalum disks, or (in case of samples for α-particle and spontaneous-fission counting) by electrodeposition. The α-particle spectra showed resolutions of typically 0.5–1% [full width at half maximum (FWHM)].

A cryosystem for the condensation and detection of very volatile α-particle and spontaneous fission activities was also applied [24]. Here, the reaction products were continuously transported by a gas jet from the target area to the detector unit. Volatile species were condensed on a solar cell kept at $\approx$40 K by a cryogenic pump. This system was used to detect Rn isotopes and was instrumental in dedicated searches for very volatile superheavy elements in the reactions $^{238}\mathrm{U} + {}^{238}\mathrm{U}$ [16] and $^{238}\mathrm{U} + {}^{248}\mathrm{Cm}$ [17].

C. Radioactivity measurements

The activity of each product was determined by observing its characteristic γ-ray transitions and/or α-particle energies. In a few cases, spontaneous fission decay of the product or its daughter was also used for identification and cross-section determination. γ-ray spectra were recorded with 5 Ge(Li) diodes of 11–27% efficiency relative to NaI and 1.8–2.35-keV resolution (FWHM) at 1332 keV. The photoelectric efficiency of the detectors as a function of source position and γ-ray energy was known to an accuracy of $\pm 3\%$. The γ-ray spectra of the various chemical fractions in the energy range 50 keV $\leqslant E_\gamma \leqslant$ 2 MeV were measured periodically at 0.5 keV/channel as a function of time for a typical period of 1 month.

α-particle spectra and spontaneous-fission events were recorded using 300 mm^2 and 450 mm^2 surface barrier detectors with absolute efficiencies of $(23 \pm 3)\%$ and $(33 \pm 3)\%$, respectively. The α-particle spectra in the energy range 2.7 MeV $\leqslant E_\alpha \leqslant$ 12.5 MeV were measured continuously at 10 keV/channel with increasing counting intervals for total periods of several months. In the cryosystem, an annular surface-barrier detector was placed in front of the solar cell. Fission fragments and their energies were recorded by coincidence signals from both detectors, whereas α-particle spectra were measured with the surface-barrier detector. Half-lives down to a few seconds could be covered as was shown by the detection of short-lived Rn isotopes.

D. Treatment of spectral data

γ-ray spectral data were analyzed with an interactive version of the code GAMANAL [25]. The data were further reduced with a set of programs using graphical display facilities making use of information "external" to a given γ-ray spectrum such as the chemical separations occurring in the preparation of the sample, available information about parent-daughter decay relationships, half-life, and γ-ray intensities in the decay of the nuclide under investigation. The decay data were analyzed in terms of known nuclides contained in a γ-ray library [26] broken into subsets consisting of the nuclides possibly present in a given sample. Thus, the assignments of a γ-ray peak and its intensity to a specific isotope was made on the basis of the chemical fraction in which it was observed, its half-life, γ-ray energy, parent-daughter relations, and corroboration by accompanying γ-ray peaks with the proper energies, half-lives, and intensities.

α-particle spectra were analyzed by simple peak integration without the use of automated fitting procedures but, whenever necessary, with a proper background subtraction. The decay data were again analyzed by least-squares minimizations in terms of known nuclides with the assignments being based on similar criteria as given above.

The decay rates were corrected for the variation of the beam intensity during the bombardment. Iterative corrections [28] owing to precursor decay during bombardment and between the end of bombardment and the chemical separation were also applied. Cross sections were calculated from the corrected activities, the chemical yields, the effective target thickness, and the beam intensity. The estimated errors in the cross sections are $\pm 3\%$ in the counting efficiencies, typically $\pm 5\%$

in the chemical yields, ±5% for the beam integration, and the statistical uncertainty obtained in the decay-curve analyses by least-squares minimization.

III. RESULTS

A. The $^{238}U + ^{238}U$ reaction

1. Isotope distributions at fixed Z below Z = 92

The integral cross sections (integrated over all values of total kinetic energy loss) for individual isotopes of a given element Z are used to define a Gaussian distribution

$$P(A;Z) = \frac{P(Z)}{[2\pi\sigma^2(A;Z)]^{1/2}} \exp\left[\frac{(A-\bar{A}_Z)^2}{2\sigma^2(A;Z)}\right] \quad (1)$$

for each Z, where $\sigma^2(A;Z)$ denotes the variance of the mass distribution at that given Z, $\bar{A}_Z$ is the centroid of the experimental distribution, and $P(Z)$ is the element yield obtained from integrating over all masses. Both $\sigma^2(A;Z)$ and $P(Z)$ vary smoothly with Z. The assumption of Gaussian distributions and smoothly varying parameters is justified by the data themselves and by similar observations in previous studies of product distributions from damped heavy-ion collisions and the associated sequential fission processes [28–33]. As an example, we show in Fig. 1 isotope yields normalized

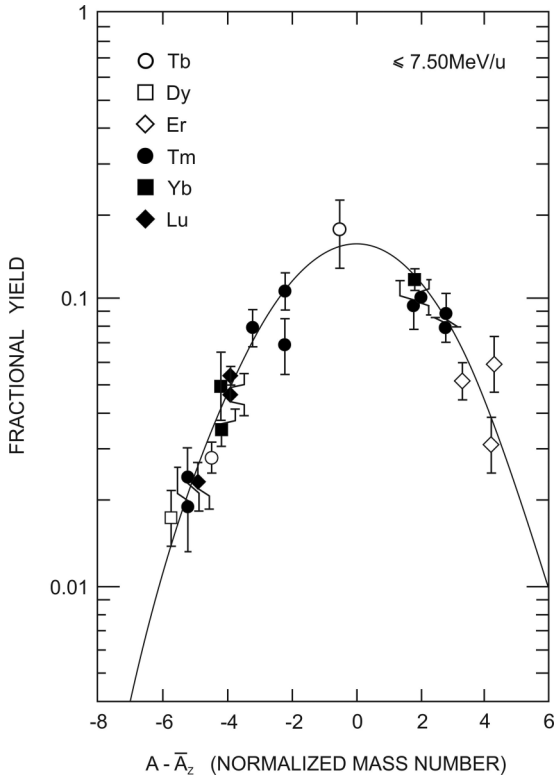

FIG. 1. Fractional independent yields at constant atomic number Z for heavy lanthanides for ⩽7.50 MeV/u $^{238}U + ^{238}U$ vs mass number A normalized to the respective centroid $\bar{A}_Z$ of the isotope distribution. The data are compatible with a single Gaussian distribution (solid line) constituted by products from the mass-symmetric fission of highly excited uraniumlike fragments. Some data have been determined twice in separate experiments.

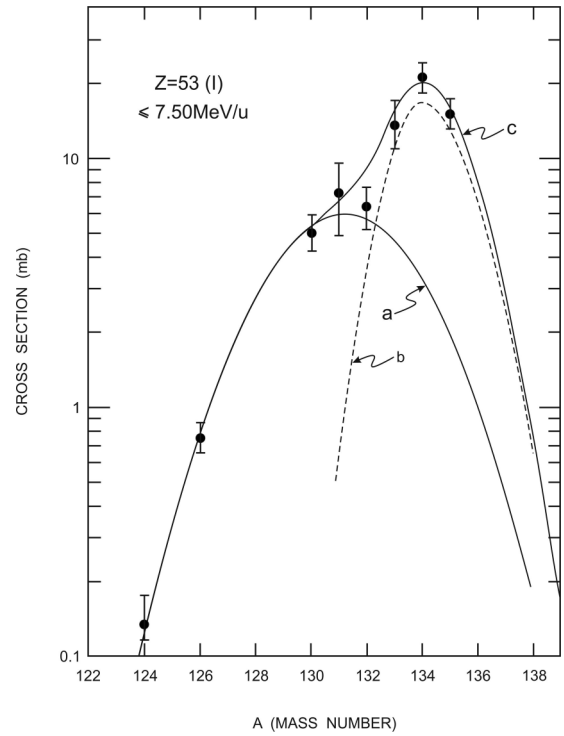

FIG. 2. Independent yields for iodine isotopes ($Z = 53$) vs mass number A for ⩽7.50 MeV/u $^{238}U + ^{238}U$. Curve a represents the yield distribution associated with fission of highly excited uraniumlike fragments. Component b is constituted by neutron-rich fission products from moderately excited uraniumlike fragments after quasielastic collisions giving rise to a double-humped fission product mass distribution where iodine is one of the main constituents of the heavy mass peak. Curve c represents the sum of components a and b.

to the respective element yield $P(Z)$ for a number of heavy lanthanide elements representing typical fission products from the mass-symmetric fission of highly excited uraniumlike fragments. For fission products with atomic numbers $33 \leqslant Z \leqslant 43$ and $50 \leqslant Z \leqslant 61$, the yield distributions are incompatible with a single Gaussian. Here, in agreement with previous results in ^{40}Ar-, ^{56}Fe-, ^{84}Kr-, and ^{136}Xe-induced reactions with ^{238}U targets, an additional component [30–33] is observed in the isotope distributions. This component is characterized by much narrower widths and more neutron-rich centroids $\bar{A}_Z$ compatible with its assignment to sequential fission of moderately excited uraniumlike fragments from quasielastic collisions giving rise to a double-humped fission-product mass distribution. Figure 2 shows the isotope yields for iodine ($Z = 53$) which is one of the main constituents of the heavy-mass peak. It depicts a decomposition of the isotope yields into a component (a) representing sequential fission of highly excited binary fragments from deep inelastic collisions and a component (b) from fission after quasielastic collisions. Both components have to be seen as the result of a superposition of the fission-product yield distributions of a number of individual fissioning nuclei of varying primary mass and charge so that the resulting integral fission product distributions are broader both in Z and A than the fission product distribution of any of the individual fission channels. Also, the expected continuous

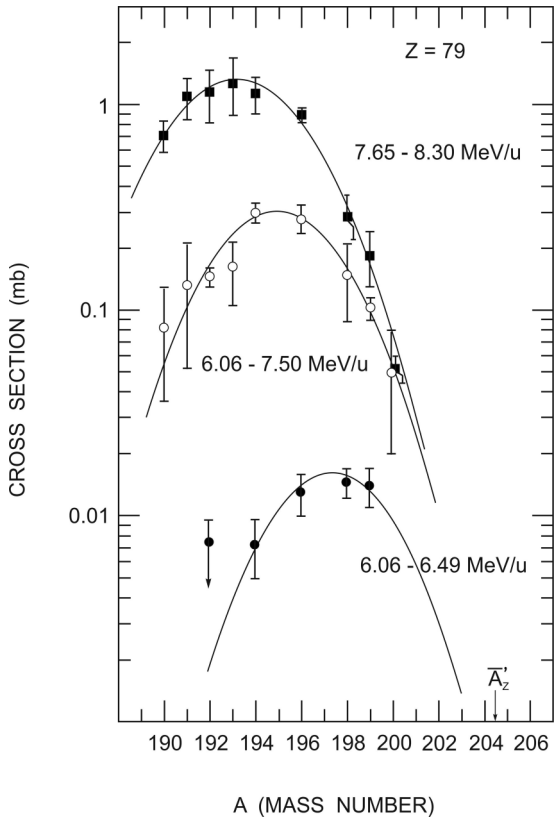

FIG. 3. Independent yields of gold isotopes ($Z = 79$) for $^{238}\mathrm{U} + ^{238}\mathrm{U}$ vs mass number A at three bins of laboratory energies (in MeV/u) defined by the incident projectile energy and the effective target thickness. The arrow marks the most probable primary mass number $\bar{A}'_Z$ calculated by minimization of the potential energy [29] of two touching liquid drops; see text.

dependence of the primary fragment cross sections on energy loss introduces another variance in the widths $\sigma^2(A;Z)$ and the centroids $\bar{A}_Z$ of the fission product distributions. Despite this broadening, there is a significant structure in the yields in the two regions of atomic numbers that are typical for fission products from low-energy fission of actinides. The fact that these processes stand out so clearly suggests that the partial cross section for collisions with small energy damping is quite large. This is discussed in more detail in Secs. III A2 and III A3. It is noteworthy that Freiesleben *et al.* [6] derived very similar conclusions with respect to the magnitude of the quasielastic cross section ($Q < -25$ MeV) from an analysis of on-line counterdata.

Another interesting feature to be discussed in the presentation of isotope distributions at fixed Z is their dependence on the bombarding energy. In Fig. 3, mass distributions for gold isotopes ($Z = 79$) representing the survivors of deep-inelastic collisions are shown for three different bins of projectile energies; see Table I. The following observations can be made.

(i) The integral cross sections depend sensitively on the projectile energy. This has important consequences for the bombarding-energy dependence of the width of the overall element distribution around $Z = 92$; see Sec. III A3.

(ii) The centroids $\bar{A}_Z$ of the postneutron emission isotope distributions are shifting to lower mass numbers as the bombarding energy increases. The mass difference between the average preneutron emission mass number $\bar{A}'_Z$ [which is calculated by minimizing the potential energy for two touching fragments (see Sec. III A2 b)] and the experimental $\bar{A}_Z$ can be associated with the average number of evaporated neutrons $\bar{\nu}_Z$. In the energy bin 6.06–6.49 MeV/u, this number is 7.1; in the energy bin 6.06–7.50 MeV/u, it is 9.5; and in the energy bin 7.65–8.30 MeV/u, it is 11.2, demonstrating that the average dissipated energy increases significantly with increasing incident projectile energy. We use this information to estimate the average total kinetic energy loss associated with the formation of these products.

(iii) The width of the isotope distributions is an increasing function of the projectile energy. These distributions are a convolution [34] of the presumably narrow primary isotope distribution by neutron-evaporation processes. Thus, the increasing widths reflect that the spectrum of energy losses associated with the formation of primary $Z = 79$ fragments broadens as the incident energy is increased. Similar observations concerning the moments of the postneutron emission isotope distributions at fixed Z as a function of bombarding energy were reported [35] for the $^{132}\mathrm{Xe} + ^{197}\mathrm{Au}$ reaction.

The large number of measured yields is used to define a surface of independent yields in the two-dimensional Z-A plane. The process used to generate the surface was discussed in detail in Refs. [28,30]. Interpretations of the resulting yield surface in terms of reaction mechanisms are discussed in the following paragraphs.

2. *The element distribution at* $\leqslant$*7.5 MeV/u*

A rather complete yield surface between atomic numbers 23 and 100 including isotopes with half lives from 23 min to 7.4×10^3 yr was obtained for the bombardment of a thick uranium targets with 7.50 MeV/u ^{238}U ions; see Table I. The results [7] are displayed in Figs. 4(a) and 4(b). Note here that the cross sections presented in our previous publication [7] were "integral cross sections" for projectilelike plus targetlike products. Apart from the data contained in Figs. 4(a) and 4(b), the cross sections for the reaction $^{238}\mathrm{U} + ^{238}\mathrm{U}$ presented throughout this paper have been divided by a factor of 2 to make them compatible with the cross sections in the $^{238}\mathrm{U} + ^{248}\mathrm{Cm}$ reaction where the yields for $Z < 92$ are projectilelike, and the yields for $Z > 92$ are targetlike, to a good approximation. The systematics of yield dispersions suggest to interpret the distribution as being attributable to a superposition of four components.

a. Quasielastic transfer residues. Products in the closest vicinity of ^{238}U originate predominantly from quasielastic pickup and stripping processes (preferentially of neutrons) and exhibit very narrow widths $\sigma^2(A;Z) \approx 1$ and centroids $\bar{A}_Z$ that are close in their A/Z ratios to A/Z of ^{238}U. The distinction of this component from the damped collision products is not as clear as in the $^{132}\mathrm{Xe} + ^{197}\mathrm{Au}$ reaction [28,35] where

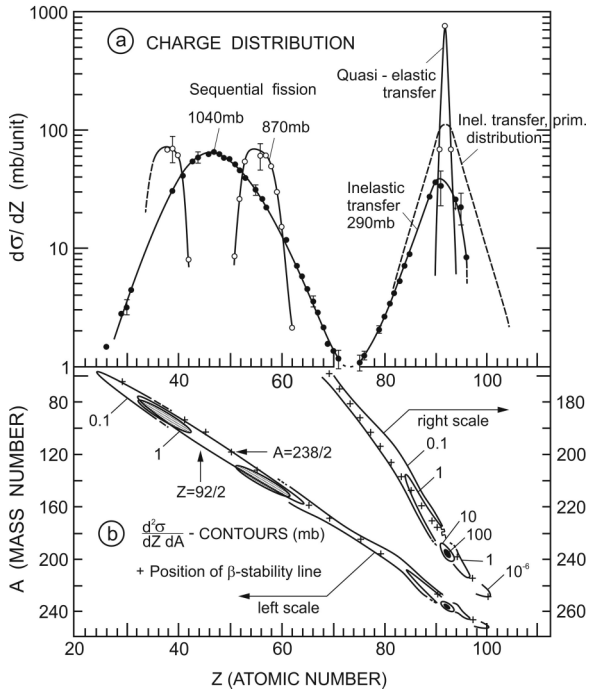

FIG. 4. Element distribution for $\leqslant$7.50 MeV/u ^{238}U + ^{238}U. (a) Yields for quasielastic transfer and sequential fission at low excitation energies (open symbols) and for damped collisions with the associated sequential fission process (solid circles). The dashed line represents the reconstructed primary yield distribution for the damped collision process. (b) Independent yield isopleths in the *Z*-*A* plane. The location of the ß-stability line is indicated for comparison. Adapted from Schädel *et al*. [7].

the different behavior of the 2^- ground states and the 12^- isomeric states of ^{196,198,200}Au with respect to their yields and the associated energy losses provided strong arguments for a distinction of quasielastic and damped collision processes. The integral cross section for quasielastic transfer, which is mainly contributed by ^{237}U and ^{239}U, is 890 $\pm$ 180 mb [7].

b. Deep-inelastic transfer residues. This component includes products with $Z \approx 73$ through $Z = 100$ arising from an originally symmetric distribution associated with binary inelastic collisions. The survivors of this reaction channel constitute an integral cross section of 290 $\pm$ 50 mb [7]. The maximum of the surviving products is close to $Z = 91$ rather than at $Z \approx 80$ or 85 as observed in the ^{84}Kr + ^{238}U and ^{136}Xe + ^{238}U reactions [32,33], respectively. Apparently, the fission competition which truncates the original fragment distribution is less important in the ^{238}U + ^{238}U system. Qualitatively similar conclusions were derived from counterexperiments [5,6] which suggest that given elements in the uranium environment are produced at smaller average excitation energies in ^{238}U + ^{238}U collisions than in other reactions. The yield contours near $Z = 92$ in Fig. 4(b) indicate clearly that the yield locus $\bar{A}_Z$ in the *A*-*Z* plane relative to the line of ß stability gradually shifts from neutron rich nuclei to more and more neutron-deficient species as the amount of charge transfer (and the associated average energy loss) increases. Table II summarizes data for the experimental centroids $\bar{A}_Z$ and for model predictions of the most probable primary mass numbers $\bar{A}'_Z$ based on the minimization of the potential energy of the dinuclear system at the scission point.

Assuming that the intermediate complex is composed of two touching spherical nuclei, one can calculate for each mass asymmetry the potential energy of the system as a function of Z as

$$E_{\rm pot} = E(A'_l; Z_l) + E(A'_h; Z_h) + \frac{Z_l Z_h e^2}{R} + V_N(R) + \frac{l(l+1)\hbar^2}{2\mu R}. \quad (2)$$

The first two terms are the liquid-drop energies of the two primary fragments followed by the Coulomb, nuclear, and centrifugal potential. The minimum-potential energy (MPE) concept is justified by phase space considerations relating the most probable transfer with the highest level density in the intermediate complex. The highest level density is associated with the maximum available energy E^* (or the minimum potential energy) in the dinuclear system. ΔE^* can be calculated from Eq. (2) if the potential energy is normalized to the entrance channel potential energy. Then, the change in liquid-drop energies between entrance and exit channel is the conventional ground-state Q value, $Q_{\rm gg}$, and

$$\Delta E^* = Q_{\rm gg} + \Delta V_C + \Delta V_N + \Delta V_l - \delta n - \delta p, \quad (3)$$

where δn and δp are corrections of the available energy owing to breaking of neutron and proton pairs in the diffusion process [27]. Omission of these corrections would correspond to the unrealistic assumption that nucleons are transferred from the ground state of the donor nucleus to the ground state of the acceptor nucleus which would lead to an overestimate of the available energy ΔE^* and consequently to an overestimate of the level density in the intermediate complex. In practice, for the prediction of mass distributions at fixed Z, δp can be omitted, whereby Eq. (3) is termed Volkov's generalized $Q_{\rm gg}$ systematics including nonpairing corrections δn. $\Delta E^*(Z)$ can then be used to estimate the average number of evaporated neutrons $\bar{\nu}_Z$. These data make it possible to estimate the average fragment excitation energies $\bar{E}_Z$ with the help of statistical neutron-evaporation calculations [36], which were performed for several isotopes with primary mass numbers A'_Z close to the predicted centroid $\bar{A}'_Z$. The average number of neutrons being emitted at a given excitation energy and angular momentum from each primary fragment can be approximated by the linear dependence [34],

$$\bar{\nu}_Z = \beta \bar{E}_Z + \gamma, \quad (4)$$

where $\beta = 1/e$, with e being a nearly constant energy carried away by each evaporated neutron. γ represents a minimum excitation energy for which no additional neutron is evaporated. The values of e and γ are determined from evaporation calculations. The value of γ is dependent on angular momentum. Here, systematic uncertainties are introduced because the angular momenta can only be predicted theoretically. We chose a fragment spin of 20$\hbar$ derived from the average orbital angular momentum in the thick target [13]. The uncertainties in $\bar{\nu}_Z$ introduced by varying the angular momenta between 10$\hbar$ and 30$\hbar$ combined with another uncertainty of 0.5 mass units in

TABLE II. Experimental centroids $\bar{A}_Z$ of the Gaussian isotope distributions at fixed Z of the light fragment for $\leqslant$7.50 MeV/u ^{238}U + ^{238}U. Model predictions [29] for the most probable primary mass numbers $\bar{A}'_Z$, the deduced average number of evaporated neutrons $\bar{\nu}_Z$, and the associated excitation energies $\bar{E}_Z$ are listed as well. These are used to calculate the total excitation energies $\bar{E}_{\rm tot}$ and the average total kinetic energy loss $\overline{\rm TKEL}$.

Experimental		Calculated quantities				
$Z_{\rm l}$	$\bar{A}_Z$	$\bar{A}'_Z$[a]	$\bar{\nu}_Z$	$\bar{E}_Z$(MeV)[b]	$\bar{E}_{\rm tot}$(MeV)[c]	$\overline{\rm TKEL}$(MeV)[d]
91	233.0	235.4	2.4	19	39	41
90	229.5	232.8	3.3	28	57	59
89	226.0	230.2	4.2	35	72	75
88		227.7				
87		225.1				
86		222.5				
85	212.3	219.9	7.6	68	148	153
84	208.7	217.3	8.6	77	168	172
83	205.6	214.7	9.1	82	182	187
82	202.3	212.1	9.8	88	197	202
81	199.7	209.5	9.8	92	209	215
80	197.3	207.0	9.7	95	218	226
79	194.9	204.4	9.5	95	221	231

[a]Obtained by minimization of the potential energy for two touching spherical liquid drops (no shell correction). The potential includes a contribution from the Coulomb and nuclear potential (proximity theory) at a fixed distance of the charge centers of $R = 14.6$ fm.
[b]Based on statistical evaporation calculations with the code ALICE [26] for an average fragment spin of 20$\hbar$ [13].
[c]Deduced from $\bar{E}_Z$ with the assumption of a sharing of the total excitation energy in proportion to the primary masses (equal temperature concept).
[d]Calculated from $\bar{E}_{\rm tot}$ using the ground-state Q value, $Q_{\rm gg}$, for the most probable primary mass number.

the predicted value of $\bar{A}'_Z$ result in an uncertainty on the order of 10 MeV in $\overline{\rm TKEL}$. The values of $\overline{\rm TKEL}$ in Table II have been derived by assuming partition of the total excitation energy in proportion to the fragment masses and by taking into account the ground-state Q value, $Q_{\rm gg,}$, for the most probable mass split. Figure 5(a) depicts the calculated most probable primary mass numbers $\bar{A}'_Z$ together with the experimental centroids $\bar{A}_z$ and the resulting differences $\bar{\nu}_Z$. In Fig. 5(b), we show the resulting average total excitation energies, $\bar{E}_Z$, deduced from $\bar{\nu}_Z$ and the values of $\overline{\rm TKEL}$ by taking into account the values of $Q_{\rm gg}$. In Fig. 6, we compare our values of $\overline{\rm TKEL}$ with those of Refs. [5,6]. Both sets of data refer to the residues of deep-inelastic collisions and are, thus, modified by sequential fission. For small charge transfers, the values of $\overline{\rm TKEL}$ of this work are typically about 30 MeV lower than in the thin-target experiment with the difference decreasing with increasing charge transfer developing into even slightly larger values in the thick-target experiment for the largest charge transfers. This reflects a genuine difference between the thin-target experiment [5,6] and the present thick-target experiment: In the present study, for the largest charge transfers, the thick-target cross sections are dominated by contributions from the highest bombarding energy bins inside the thick target; see Fig. 3. The relative contribution by lower bombarding energy bins to the thick-target cross section is expected to increase notably for the smaller charge transfers. At lower bombarding energies, the available energy above the barrier is smaller and the average dissipated energy associated with the formation of a given product in the vicinity of the entrance channel charge is reduced. Thus, the data in Fig. 6 show the expected trend which supports the validity of the method used to deduce $\overline{\rm TKEL}$ in this work.

c. Sequential fission after quasielastic collisions. As mentioned above, we have evidence for the presence of a double-humped fission product mass distribution which is assumed to include all fission processes occurring in the deexcitation of low or moderately excited primary fragments from quasielastic collisions. In an attempt to fit both the mass and the charge yields of this component with known fission yield systematics of neutron-induced fission reactions, we found a reasonable agreement with the data for the ^{239}Pu($n_{14\ \rm MeV}, f$) reaction [37]. Lower atomic numbers of the fissioning nuclei such as ^{235}U and lower excitation energies as in the ^{235}U($n_{\rm th}, f$) reaction were found to be less compatible with experiment. This may indicate that the fissioning nuclei are, on the average, the product of the transfer of one or a few charges to one of the ^{238}U nuclei. The integral cross section for the double-humped fission product distribution is 870 ± 210 mb [7].

d. Sequential fission after deep-inelastic collisions. The massive, nearly symmetric fission product distribution [Fig. 4(a)] is assumed to originate from sequential fission of highly excited binary inelastic fragments and has an integral cross section of 1040 ± 200 mb [7]. The centroid of this distribution is close to $Z = 47$, $A = 116$. If no charged-particle evaporation occurs in the sequential fission of the primary fragments, again $_{94}$Pu can be seen as the most probable fissioning system. If the neutron-to-proton degree of freedom is relaxed in the first reaction step, the most probable primary mass number associated with Pu will be $\bar{A}'_Z = 242$. The mass balance then requires the assumption

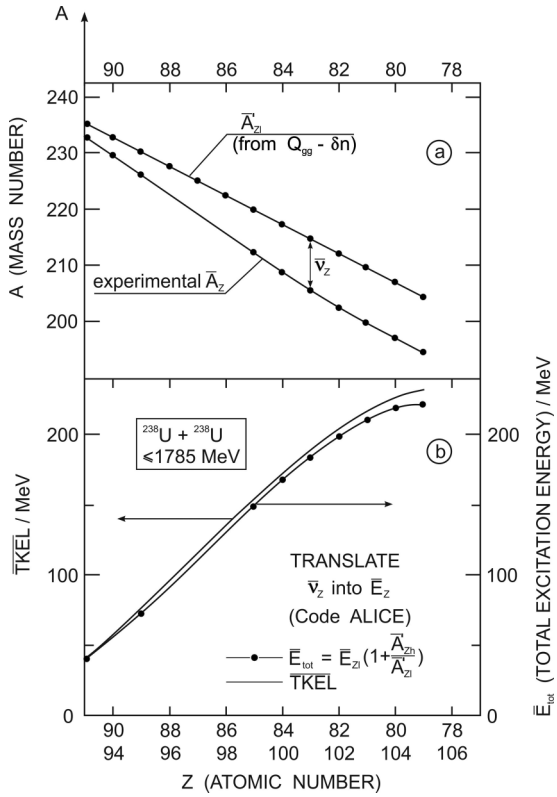

FIG. 5. (a) Primary mass numbers $\bar{A}'_Z$ for the light uraniumlike fragments for $Z \leqslant 91$ obtained by minimization of the potential energy for two touching spherical liquid drops (no shell correction) including corrections δn for the breaking of neutron pairs in the nucleon exchange process. Comparison with the experimental mean product mass number $\bar{A}_Z$ for $\leqslant$7.50 MeV/u $^{238}\mathrm{U} + ^{238}\mathrm{U}$ gives the average number of neutrons $\bar{\nu}_Z$ evaporated from the primary fragments. (b) Their mean excitation energy $\bar{E}_Z$ is shown as determined with a statistical evaporation code. The mean total excitation energy $\bar{E}_{\mathrm{tot}}$ as a function of Z is indicated involving the assumption of a partition of the excitation energy between complementary fragments in proportion to their primary masses. The values of the total kinetic energy loss $\overline{\mathrm{TKEL}}$ result from $\bar{E}_{\mathrm{tot}}$ by adding Q_{gg}.

that a total of ten neutrons are evaporated on the average. For events with larger-than-average energy damping in the first reaction step, this number can be considerably higher. This will lead to very neutron-deficient fission products such as the α-particle emitters ^{149}Tb and ^{148}Gd, which have been observed experimentally.

e. Total reaction cross section. By adding the residual and the corresponding fission component cross sections of both the quasielastic and the damped reaction products, the total reaction cross section can be derived in a direct manner. One must take into account that two or even four fragments arise from a single collision. If the sum rule emerging from this consideration is taken into account, one obtains a total reaction cross section of 1067 ± 217 mb. This is to be compared with the expected thick-target cross section

$$\bar{\sigma}_r = \pi R^2 \frac{\int_B^E \left(1 - \frac{E}{B}\right) dE}{(E - B)}, \tag{5}$$

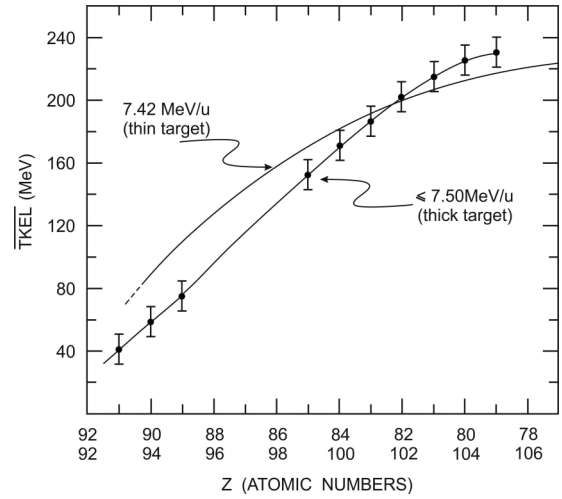

FIG. 6. Average values of the total kinetic energy loss $\overline{\mathrm{TKEL}}$ from Fig. 5 and Table II with estimated uncertainties of $\approx$10 MeV vs atomic number of the binary inelastic fragments. The uncertainties result from reasonable variations in the model parameters in the potential energy and statistical evaporation calculations; see text. The solid line represents the Z dependence of the average kinetic energy loss in the thin-target experiment at 7.42 MeV/u [5].

which for an interaction radius (quarter-point radius of $R = 16.89$ fm [1] results as 920 mb. There is agreement within the uncertainty limits.

f. Reconstruction of the primary deep-inelastic distribution. To deduce the primary charge distribution for the damped collision process, we use its integral cross section of 405 ± 75 mb (the sum of the cross sections for the residual distribution and the symmetric fission distribution), assume the distribution to be symmetric around $Z = 92$ and to have the usual shape as found, e.g., in the Xe + Au reactions [28]. The width of the distribution is adjusted to the measured element yields near $Z = 80$, where fission probability is negligible [5]. The resulting primary distribution is shown as a dashed curve in Fig. 4(a).

The beam energy ("effective energy" [20]) at which the reaction cross section is equal to the thick-target cross section $\bar{\sigma}_r$ is 7.0 ± 0.2 MeV/u, which is lower than the beam energy of 7.42 MeV/u used in Refs. [5,6]. Nevertheless, if one compares partial cross sections relative to $\bar{\sigma}_r$, a meaningful comparison with the results of Refs. [5,6] and of this work is possible; see Table III. Both experiments give a comparatively large fraction of quasielastic reaction products. The lower effective energy of the present work seems to result in a noticeable preference for these quasielastic channels. This tendency is further enhanced at even lower bombarding energies, as we see in Sec. III A3.

Table III shows that the fractions of surviving products in the deep-inelastic channels relative to both the reconstructed primary deep-inelastic cross section and to the total reaction cross section are almost the same.

3. Bombarding energy dependence of the deep-inelastic product distribution

In addition to the measurement of the element distribution at 7.50 MeV/u, such measurements were also performed for

TABLE III. Partial cross sections (mb) in the $^{238}U + ^{238}U$ reaction.

	This experiment $\leqslant$7.50 MeV/u (thick target) effective energy 7.0 ± 0.2 MeV/u	Freiesleben *et al.* [6] 7.42 MeV/u (thin target)
Reaction cross section σ_r	1067 ± 217	1630 ± 1
Deep-inelastic reaction primary distribution DIR_{prim}	405 ± 75	800 ± 50
Deep-inelastic reaction residual distribution DIR_{res}	145 ± 25	280 ± 30
Quasielastic reaction primary distribution QER_{prim}	662 ± 142	830 ± 100
QER_{prim}/σ_r	0.62 ± 0.13	0.51 ± 0.07
DIR_{prim}/σ_r	0.38 ± 0.10	0.49 ± 0.07
DIR_{res}/DIR_{prim}	0.36 ± 0.09	0.35 ± 0.04
DIR_{res}/σ_r	0.14 ± 0.04	0.17 ± 0.03

elements with $68 \leqslant Z \leqslant 100$ at 6.49 and 8.30 MeV/u, respectively. The target thicknesses (see Table I) define ranges of projectile energies $B \leqslant E \leqslant 6.49$ MeV/u, $B \leqslant E \leqslant 7.50$ MeV/u, and $7.65 \leqslant E \leqslant 8.30$ MeV/u covered inside the targets. Isotope distributions for gold ($Z = 79$) at these three energy bins are shown in Fig. 3. Integration of these Gaussian distributions at fixed Z gives the element yields shown in Fig. 7. The most striking feature of the data is the large reduction in the deep-inelastic product cross section for the lowest energy bin. Large reductions in the mass and charge diffusion at near-barrier energies have previously been reported [28,38,39]. Moreover, in contrast to experiments at higher bombarding energies, studies at near-barrier energies have revealed evidence [39] for a strongly nonlinear evolution of the mass and charge variances as a function of the interaction time. Attempts to reproduce the observed energy dependence with a phenomenological treatment of mass diffusion are discussed in Sec. IV. As the fission product distribution has not been measured at the 6.49 and 8.30 MeV/u experiments, reconstruction of the primary distribution of the deep-inelastic products in these two cases is only possible approximately: The shape of that distribution is assumed to be similar to the dashed line in Fig. 4(a). The width of the distributions is again fixed at $Z \leqslant 80$, where sequential fission is assumed to be negligible at all incident energies. It is further assumed that the primary yields for $Z \geqslant 80$ are increasingly depleted by sequential fission for increasing atomic numbers and increasing incident energies. The resulting estimates of the relative contribution of deep-inelastic collisions to the total reaction cross sections are then

$$DIR_{prim}/\sigma_r \approx 0.20 \quad \text{at} \quad B \leqslant E \leqslant 6.49 \text{ MeV/u}$$

and

$$DIR_{prim}/\sigma_r \approx 0.55 \quad \text{at} \quad 7.65 \leqslant E \leqslant 8.30 \text{ MeV/u}.$$

Together with the ratios given in Table III for $B \leqslant E \leqslant 7.50$ and 7.42 MeV/u, these estimates indicate that quasielastic collisions are the most dominant reaction mechanism near the barrier and that their relative importance decreases continuously as the beam energy is increased. In terms of absolute cross sections, this means that the cross

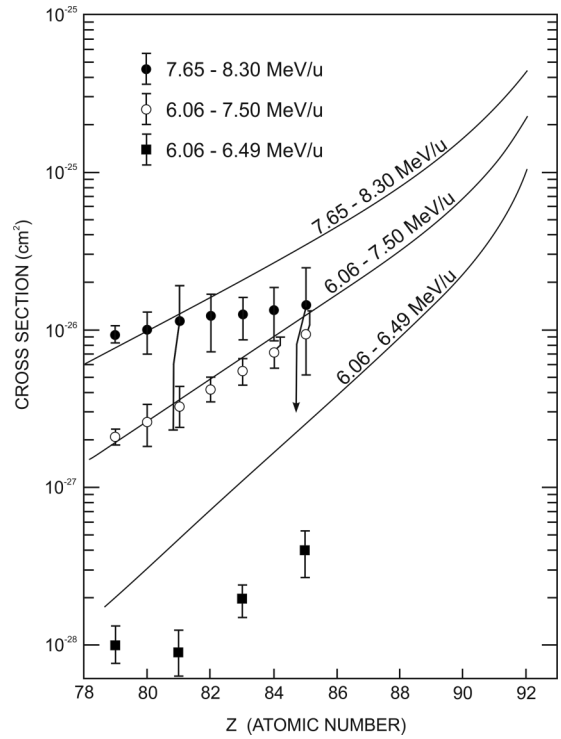

FIG. 7. Element yields $P(Z)$ of uraniumlike fragments in three different bins of laboratory energies (in MeV/u) defined by the incident projectile energy and the effective target thickness. For the higher energy bins and for the higher atomic numbers, the data (representing cross sections for the survivors of the deep-inelastic collisions) are increasingly depleted by sequential fission. The solid lines are the results of diffusion-model predictions [13]; see Sec. IV.

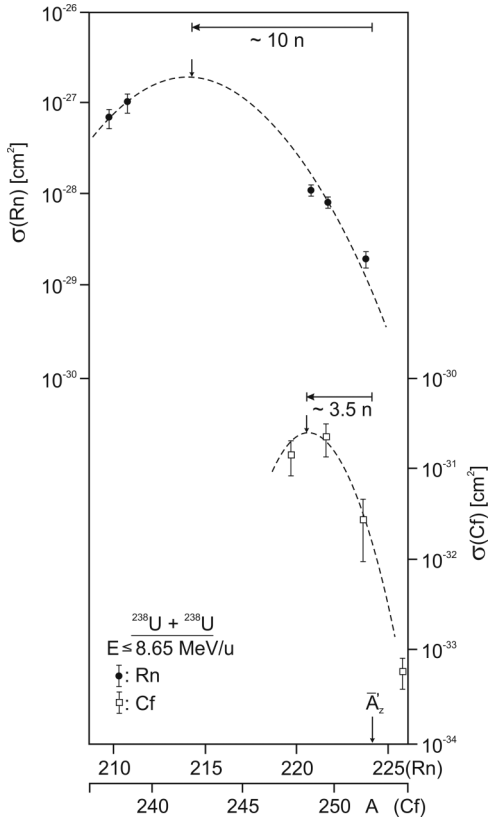

FIG. 8. Isotope distributions of the complementary elements $_{86}$Rn and $_{98}$Cf in the ^{238}U + ^{238}U reaction at $\leqslant$8.6 MeV/u. $\bar{A}'_Z$ is the most probable primary mass number calculated within the generalized Q_{gg} systematics including corrections for the breaking of neutron pairs.

section for the damped collision process rises steeper with increasing incident energy than the total reaction cross section. Consequently, for reactions with very large mass transfer, e.g., for the reaction

$$^{238}\mathrm{U} + {}^{238}\mathrm{U} \rightarrow {}_{114}\mathrm{X} + {}_{70}\mathrm{Yb},$$

for which a cross section of 10^{-28} cm^2 can be extrapolated from the data at $\leqslant$7.50 MeV/u (see below, Fig. 16), the cross sections are dramatically reduced at near-barrier energies. At $B \leqslant E \leqslant 6.49$ MeV/u, the primary yield for $Z_h = 114$, $Z_l = 70$ is of the order of 10^{-30} cm^2 only. The folding of this primary yield with estimated Γ_n/Γ_f values for the emission of three neutrons leads to estimates of the cross sections for evaporation residues of 10^{-39} to 10^{-40} cm^2 which are not accessible experimentally.

4. *Isotope distributions at fixed Z above Z = 92*

As an example, isotopic distributions of the complementary elements Rn and Cf from the ^{238}U + ^{238}U reaction at a bombarding energy of $\leqslant$8.65 MeV/u [16] are shown in Fig. 8. This figure is a very suitable introduction to this chapter. The arrow at $A = 224.1/251.9$ indicates the location of the most probable primary mass number calculated with the generalized Q_{gg} systematics including nonpairing corrections δn. The differences between the measured maxima $\bar{A}_Z$ and the most probable primary mass number $\bar{A}'_Z$ are a measure for the number of evaporated neutrons. For Rn, this number is $\approx$10.1 and for Cf it is $\approx$3.5, indicating extremely different average excitation energies, large dissipated energies in the case of Rn, and much lower dissipated energies in the Cf nuclei. While the integral cross section for Rn is close to the primary yield, the yield of the Cf isotopes is depleted by sequential fission by many orders of magnitude. Thus, it is evident from Fig. 8 that surviving evaporation residues of the heavy actinides are associated only with the low-energy tails of the excitation-energy distributions.

a. Results at $\leqslant$7.50 MeV/u incident energy. Isotopic cross sections for transuranium elements up to fermium ($Z = 100$) are shown in Fig. 9. Most of these cross sections are not modified by precursor decay because the isotopes are shielded or because the precursor yields are negligible. Other independent yields were derived by taking into account the growth from their precursors. In these cases, the error limits include the uncertainties introduced in the precursor correction. For a few isotopes (partially) cumulative yields are given in Fig. 9 because quantitative information on the contribution from their precursors was not available. Mendelevium isotopes ($Z = 101$) could not be detected anymore. Upper limits for their cross sections are below 10^{-33} cm^2, which corresponds to the detection limits set by the integral particle numbers of about 10^{16} particles; see Table I. For comparison, actinide cross sections were also determined in the ^{136}Xe + ^{238}U reaction using a thick target and the same incident energy of 7.50 MeV/u [40]. These data are also depicted in Fig. 9. They are very similar to ^{136}Xe + ^{238}U actinide cross sections measured at $\leqslant$8.2 MeV/u [41] and $\leqslant$8.3 MeV/u [42]. The apparently weak dependence of these thick-target cross sections on the projectile energy is consistent with the energy dependence measured in the ^{238}U + ^{238}U reaction; see Sec. III A4 b. Because of the weak energy dependence, the comparison of thick uranium-target actinide cross sections obtained with different projectiles is meaningful. The strong enhancements in the heavy actinide yields in the ^{238}U + ^{238}U reaction vs the ^{136}Xe + ^{238}U reaction are at first sight astonishing. If a given mass transfer in these reactions occurs with the same probability and is associated with the same energy loss, heavy actinide production should be favored in the ^{136}Xe + ^{238}U reaction. This is because of the much more negative Q_{gg} values in the latter reaction. For example, for $_{98}$Cf production, $Q_{gg} = -33$ MeV for ^{136}Xe + ^{238}U, whereas the total excitation energy is reduced by $Q_{gg} = -2$ MeV only with the ^{238}U projectile. Thus, the increases in the actinide cross sections with the ^{238}U projectile are to be seen as strong evidence for a much larger primary mass flow at a given dissipated energy in the ^{238}U + ^{238}U reaction. This is expected on the basis of the phase space available above the potential energy surface (PES). Ground-state Q values and the minimum of the PES for ^{136}Xe + ^{238}U and ^{238}U + ^{238}U are shown in Fig. 10. According to Schmidt and Wolschin [14] and Grossmann [15], the very flat PES for ^{238}U + ^{238}U with a minimum near $Z_h = 102$ and $Z_l = 82$ strongly influences the early development of the colliding system. Therefore, large mass transfer is favored with relatively small dissipated energies. For the early development of the ^{136}Xe + ^{238}U reaction, the dissipated energy per exchanged nucleon is 2 to 4

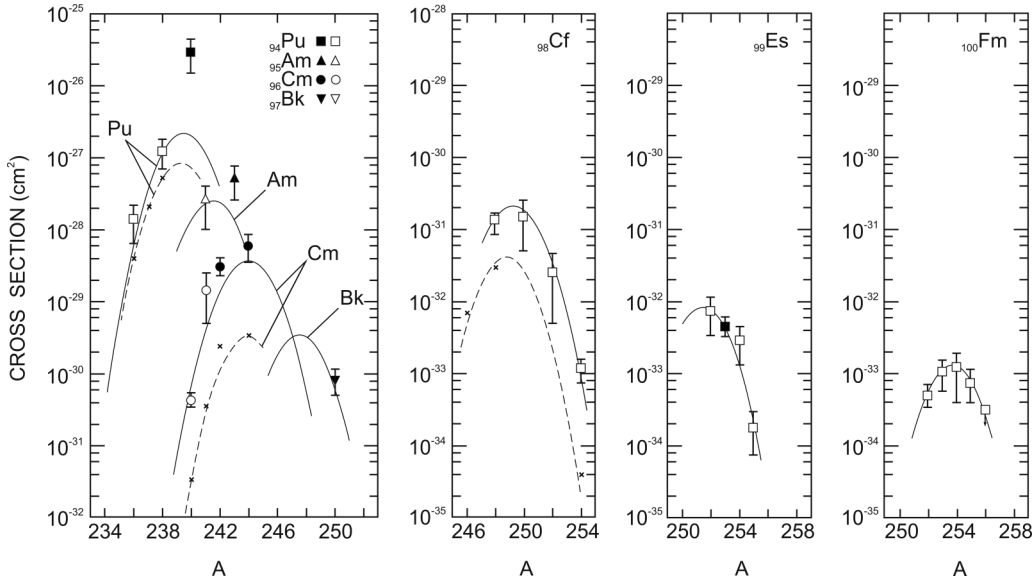

FIG. 9. Thick-target cross sections for the production of $_{94}$Pu, $_{95}$Am, $_{96}$ Cm, $_{97}$Bk, $_{98}$Cf, $_{99}$Es, and $_{100}$Fm isotopes in the ^{238}U + ^{238}U reaction at $\leqslant$7.50 MeV/u with modified data from Ref. [40] (see text). Open symbols denote independent yields, closed symbols cumulative yields. For comparison, cross sections for bombardments of thick ^{238}U targets with $\leqslant$7.50 MeV/u ^{136}Xe ions (crosses) from this work are also shown.

times higher than with the ^{238}U projectile owing to the higher energy required for particle-hole excitations which accompany the exchange of nucleons [43].

b. Results at other incident energies. To investigate the dependence of the actinide production rates on incident energy, several thick-target bombardments were carried out [40] with projectile energies varying from 6.49 to 8.65 MeV/u, as well as bombardments of relatively thin targets at 8.30 and 9.00 MeV/u, respectively; see Table I. The mean cross sections

$$\bar{\sigma} = \frac{\int_{E1}^{E2} (d\sigma/dE)dE}{(E_2 - E_1)} \tag{6}$$

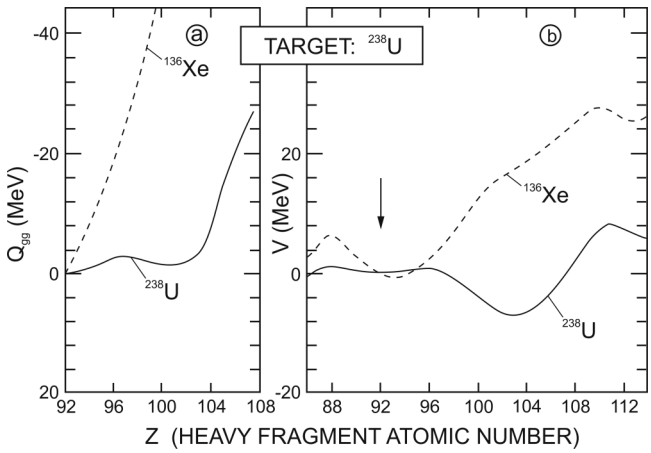

FIG. 10. (a) Ground-state Q values, Q_{gg}, associated with the formation of heavy fragments in transfer reactions of ^{136}Xe and ^{238}U projectiles with ^{238}U targets. (b) Minimum of the potential energy surface vs charge number Z of the heavy fragment for the same reactions.

for Cm, Cf, and Fm isotopes are listed in Table IV. In contrast to the mean cross sections for the light complements Ra through Bi (Fig. 7), the actinide cross sections do not increase by orders of magnitude with increasing incident projectile energy [40]. As an example, Fig. 11 shows the thick-target cross sections for Cf isotopes. The data are compatible with the same variance of the Gaussian distribution and the same centroid $\bar{A}_Z = 249.3$ at all incident energies. Similar observations hold for the other actinide elements [40]. This again is in contrast to the isotope distributions for the much less fissile complementary products near $Z = 80$, where both the widths and the centroids of the distributions depend on incident energy (Fig. 3), reflecting marked differences in the associated excitation energy spectra. Presumably, for the surviving actinides at each bin of projectile energies, only low excitation energies are involved; see Fig. 8. We can estimate these excitation energies in the following way: If we assume rapid mass and charge equilibration [29], the most probable primary masses $\bar{A}'_Z$ associated with the formation of given elements can be derived by minimization of the potential energy for two touching spheres [27–29]. Values of $\bar{A}'_Z$ for the light complements derived from this generalized Q_{gg} systematics including corrections for the breaking of neutron pairs in the mass exchange are listed in Table II. The differences between the centroids $\bar{A}'_Z$ for the complementary heavy fragments and the respective experimental centroids $\bar{A}_Z$, i.e., the average number of neutrons evaporated from the primary actinide fragments is 3 to 5, with a tendency to increase slightly from lighter to heavier actinides. If we use predicted angular momenta [13], statistical evaporation calculations yield an average excitation energy carried away per emitted neutron of about 9 MeV. Thus, we estimate average excitation energies close to 35 MeV for the survivors of the actinides in all bins of projectile energies.

c. Differential actinide cross sections versus projectile energy. The similarity of the mass distributions (Table IV and

TABLE IV. Average thick-target cross sections between the incident laboratory energy E and the interaction barrier $B = 6.06$ MeV/u for targetlike Cf through Fm products in $^{238}U + ^{238}U$ bombardments; i.e., target- plus projectilelike values from Ref. [40] are divided by 2. i, independent cross sections; c, partially cumulative cross sections.

	Thick-target cross section (cm^2)			
Isotope	$E \leqslant 6.49$ MeV/u	$E \leqslant 6.84$ MeV/u	$E \leqslant 7.50$ MeV/u	$E \leqslant 8.65$ MeV/u
^{248}Cf	$(8.5 \pm 5) \times 10^{-32}$ i	$(1.9 \pm 0.5) \times 10^{-31}$ i	$(1.35 \pm 0.25 \times 10^{-31}$ i	$(7.5 \pm 3) \times 10^{-32}$ i
^{249}Cf		$(2.0 \pm 1.5) \times 10^{-30}$ c		$(\leqslant 1.3) \times 10^{-30}$ c
^{250}Cf		$(2.15 \pm 0.45) \times 10^{-31}$ i	$(1.5 \pm 1.0) \times 10^{-31}$ i	$(1.2 \pm 0.5) \times 10^{-31}$ i
^{251}Cf		$(<2.0) \times 10^{-30}$ i		$(<4.5) \times 10^{-30}$ i
^{252}Cf		$(3.35 \pm 0.8) \times 10^{-32}$ i	$(2.5 \pm 2.0) \times 10^{-32}$ i	$(1.5 \pm 1.0) \times 10^{-32}$ i
^{254}Cf	$(6.5 \pm 5) \times 10^{-34}$ i	$(1.55 \pm 0.5) \times 10^{-33}$ i	$(1.15 \pm 0.3) \times 10^{-33}$ i	$(3.15 \pm 1.0) \times 10^{-34}$ i
^{252}Es	$(7.0 \pm 6.0) \times 10^{-33}$ i	$(8.0 \pm 5.0) \times 10^{-33}$ i	$(6.0 \pm 4.0) \times 10^{-33}$ i	$(2.25 \pm 1.25) \times 10^{-33}$ i
^{253}Es	$(6.0 \pm 2.0) \times 10^{-33}$ i	$(1.05 \pm 0.4) \times 10^{-32}$ c	$(4.5 \pm 2.0) \times 10^{-33}$ c	$(3.0 \pm 1.5) \times 10^{-33}$ c
^{254m}Es	$(1.1 \pm 0.25) \times 10^{-33}$ i	$(4 \pm 2) \times 10^{-34}$ i	$(1.05 \pm 0.35) \times 10^{-33}$ i	$(3.5 \pm 2.5) \times 10^{-33}$ i
^{254g}Es	$(\leqslant 1.0) \times 10^{-33}$ i	$(\leqslant 1.7) \times 10^{-33}$ i	$(2.0 \pm 1.0) \times 10^{-33}$ i	$(\leqslant 7.5) \times 10^{-34}$ i
^{255}Es	$(1.25 \pm 1.0) \times 10^{-33}$ i	$(5 \pm 4) \times 10^{-34}$ i	$(1.75 \pm 1.0) \times 10^{-34}$ i	$(3.0 \pm 2.5) \times 10^{-34}$ i
^{256m}Es		$(2.5 \pm 2.0) \times 10^{-34}$ i		
^{252}Fm	$(8.0 \pm 6.5) \times 10^{-34}$ i	$(3.0 \pm 3.5) \times 10^{-34}$ i	$(4.9 \pm 1.5) \times 10^{-34}$ i	$(6.0 \pm 5.0) \times 10^{-34}$ i
^{253}Fm	$(8.0 \pm 4.5) \times 10^{-34}$ i	$(1.75 \pm 0.75) \times 10^{-33}$ i	$(1.1 \pm 0.5) \times \times 10^{-33}$ i	$(1.0 \pm 0.75) \times 10^{-33}$ i
^{254}Fm	$(1.6 \pm 1.4) \times 10^{-33}$ i	$(\leqslant 6.5) \times 10^{-34}$ i	$(1.25 \pm 0.75) \times 10^{-33}$ i	$(\leqslant 1.5)x \times 10^{-33}$ i
^{255}Fm	$(7.5 \pm 5.0) \times 10^{-34}$ i	$(6 \pm 5) \times 10^{-34}$ i	$(7.5 \pm 2.5) \times 10^{-34}$ i	$(5 \pm 4) \times 10^{-34}$ i
^{256}Fm	$(1.0 \pm 0.7) \times 10^{-33}$ i	$(1.2 \pm 1.0) \times 10^{-33}$ i	$(\leqslant 3.2) \times 10^{-34}$ i	
^{257}Fm	$(<3.5) \times 10^{-34}$ c		$(< 6.5) \times 10^{-34}$ c	$(\leqslant 3.5) \times 10^{-34}$ c

Fig. 11) with respect to their centroids and widths at all incident energies suggested to sum these distributions (assuming of Gaussian shape with the same FWHM = 3.3 u) to get the total production cross section for each Z.

These cross sections are mean values between the projectile energy and the interaction barrier. By taking differences in these element cross sections between 8.65 and 7.50, 7.50, and 6.84, as well as between 6.84 and 6.49 MeV, respectively, and

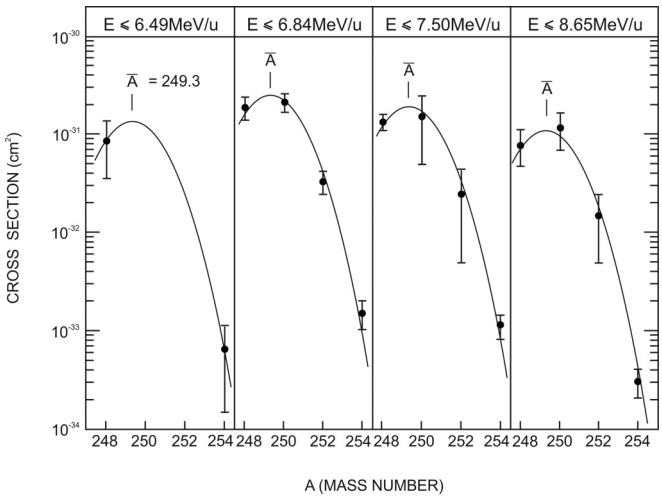

FIG. 11. Thick-target cross sections for $_{98}$Cf isotopes at four different incident energies in the $^{238}U + ^{238}U$ reaction with modified data from Ref. [40] (see text). The low-energy threshold is 6.06 MeV/u, corresponding to the Coulomb barrier, calculated with the interaction radius of 16.89 fm [5,6]. The solid lines are Gaussians centered at $\bar{A}_Z = 249.3$ at all incident energies with a constant width of 3.3 u (FWHM).

by considering the differential target thicknesses (number of target atoms) in these energy bins, we can calculate differential cross sections for each Z. Together with the results for the energy bins 7.65–8.30 MeV/u and 8.31–9.0 MeV/u, these differential element yields are listed in Table V. In Fig. 12, we show the excitation function for surviving $_{98}$Cf nuclei. There is an increase in cross section up to about 6.8 MeV/u followed by a more flat decrease at higher energies. Also shown in Fig. 12 are the cross sections determined for the complementary light element Rn. The latter cross sections have been corrected for the relatively small losses by fission and, thus, represent the primary yields for the charge split $Z_l = 86$, $Z_h = 98$ integrated over all excitation energies. The rise and fall of the $_{98}$Cf cross sections reflects the projectile energy dependence of the partial cross section contained in the low-energy part of the broad excitation energy distributions. This is discussed more quantitatively in Sec. III A4 e. The inset in Fig. 12 shows the cross sections for the residual californium nuclei relative to the integral primary cross section.

This ratio decreases exponentially with increasing projectile energies at a rate of one order of magnitude per about 0.5 MeV/u. The slope of this exponential depends on the average number of evaporated neutrons ν_i via $(\frac{\Gamma_n}{\Gamma_n+\Gamma_f})^{\nu_i}$ [cf. Eq. (8)] and hints to values between 3 and 4.

d. Analysis of the actinide cross sections at $\leqslant 7.50$ MeV/u $^{238}U + ^{238}U$. To illuminate quantitatively the mechanisms responsible for the formation of the surviving actinides, we reconstruct the measured product populations for the complementary elements $_{86}$Rn-$_{98}$Cf, $_{85}$At-$_{99}$Es, and $_{84}$Po-$_{100}$Fm with the following assumptions:

(i) The isotope distributions for the light complements $_{86}$Ra, $_{85}$At, and $_{84}$Po are not significantly influenced by fission occurring in the deexcitation of these fragments.

TABLE V. Differential cross sections (cm^2) for bins of laboratory energies E in MeV/u for targetlike fragments with atomic numbers $Z = 98$ through 100; i.e., target plus projectilelike values from Ref. [40] are divided by 2. The element yields have been obtained by integration of the respective isotopic distributions assuming Gaussian shapes and widths (FWHM) of 3.3 mass units; see text.

Element	$6.13 \leqslant E \leqslant 6.49$	$6.49 \leqslant E \leqslant 6.84$	$6.84 \leqslant E \leqslant 7.50$	$7.65 \leqslant E \leqslant 8.30$	$8.35 \leqslant E \leqslant 9.0$
Cf	$(4.7 \pm 1.3) \times 10^{-31}$	$(1.2 \pm 0.2) \times 10^{-30}$	$(5.0 \pm 2.1) \times 10^{-31}$	$(<5.6) \times 10^{-32}$	$(<9.7) \times 10^{-33}$
Es	$(3.8 \pm 1.1) \times 10^{-32}$	$(4.9 \pm 2.2) \times 10^{-32}$	$(0.8 \pm 2.5) \times 10^{-32}$	$(<1.6) \times 10^{-33}$	$(<5.8) \times 10^{-34}$
Fm	$(3.8 \pm 0.8) \times 10^{-33}$	$(4.4 \pm 1.7) \times 10^{-33}$	$(3.6 \pm 1.8) \times 10^{-33}$	$(<2.3) \times 10^{-33}$	$(<2.0) \times 10^{-34}$

(ii) The most probable mass number of primary fragments $\bar{A}'_Z$ can be deduced with the generalized Q_{gg} systematics including corrections δn for the pair breaking of the transferred neutrons [27–29]. Comparison of $\bar{A}'_Z$ with the measured mean product mass number $\bar{A}_Z$ gives the average number of neutron $\bar{\nu}_Z$ evaporated from the primary light fragments and their mean excitation energy, as calculated with an evaporation code; see Sec. III A2 b. The mean total excitation energy $\bar{E}_{tot}$ for the light and heavy fragments is deduced by assuming a partition of the excitation energy between the two fragments in proportion to their initial masses.

(iii) The measured variance for the $\sigma^2(A)$ for the isotope distributions for fixed Z results from the superposition of three dispersions:

$$\sigma^2(A) = \sigma^2(A') + \sigma^2(E^*) + \sigma^2(\nu). \quad (7)$$

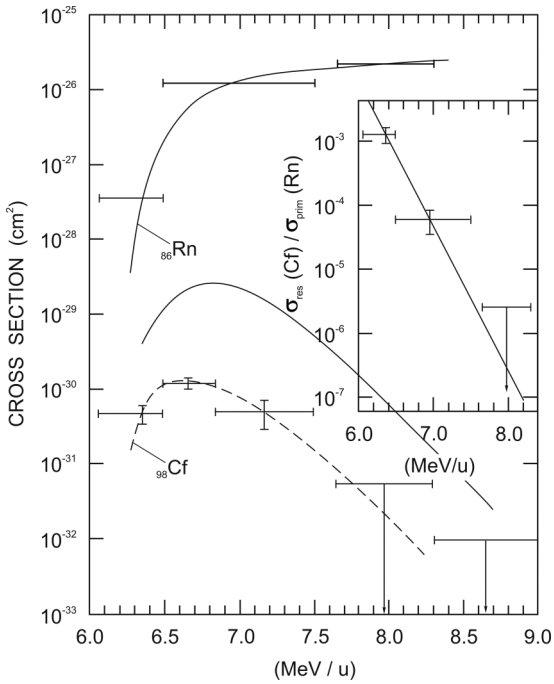

FIG. 12. Energy dependence of the production cross sections for the complementary elements $_{86}$Rn and $_{98}$Cf. The Rn yields have been corrected for a relatively small loss of yield by sequential fission and thus represent estimates for the primary yields. The Cf yields connected by the dashed line depict the shape of the excitation function for the surviving heavy actinides. The solid line results from a calculation based on the assumptions given in the text. The inset shows the survival probabilities of the $_{98}$Cf isotopes.

Here $\sigma^2(A')$ represents the variance of the primary fragment isotope distribution around $\bar{A}'_Z$, $\sigma^2(E^*)$ accounts for the broad range of total excitation energies associated with the formation of a given primary fragment A'_Z which leads to a broad range of final products A_Z in the neutron-evaporation process, and $\sigma^2(\nu)$ reflects the fluctuations in the number of evaporated neutrons from a given fragment A'_Z at fixed excitation energy.

The measured isotope distribution for polonium corresponds to $\sigma^2(A) = 6.9$ u^2. The variance $\sigma^2(\nu)$ is not larger than 0.5 u^2 in the present experiments, as follows from evaporation calculations with the code ALICE. For $\sigma^2(E^*)$, a value of $\approx$4.5 u^2 is estimated from the Q-value dispersions [5,6] of about 100 MeV FWHM. We note here that the dispersion in the excitation energy is the dominant contribution in the U + U reaction. If we neglect the dependence of $\sigma^2(A')$ and $\sigma^2(\nu)$ on excitation energy, the variance of the primary fragment isotope distributions in the Po-Fm region is $\sigma^2(A') = 2.1$ u^2 (FWHM = 3.4 u).

We can now describe the population $Y(A;Z)$ of a given actinide isotope by starting from such a narrow primary fragment distribution around the centroid $\bar{A}'_Z$, as derived from values of Q_{gg}-δn by simulating the evaporation of $\nu_i = A' - A$ neutrons:

$$Y(A;Z) = \sum_{i=1}^{k} \left(\frac{\Gamma_n}{\Gamma_n + \Gamma_f} \right)^{\nu_i} Y_i(A';Z) \cdot \int \frac{d\sigma}{dE} \cdot P(\nu_i) dE. \quad (8)$$

Here $\Gamma_n/(\Gamma_n + \Gamma_f)$ corrects for the fission competition in the evaporation chain using an empirical approach [45], based on fusion-evaporation data for light-mass projectile-induced reactions where the angular momenta of the fusion products are low. $P(\nu_i)$ (extracted from ALICE code calculations) gives the probability for the evaporation of ν_i neutrons, and $d\sigma/dE$, assumed to be Gaussian, accounts for the dispersion in excitation energy and is adjusted so as to reproduce the isotope distribution of the complementary light element. While the most abundant $_{86}$Rn, $_{85}$At, and $_{84}$Po isotopes are predominantly formed in collisions where energies close to the mean value are deposited in the system, the calculations show that the *surviving* transcurium isotopes originate exclusively from the low-energy tails of the excitation-energy distributions. In Fig. 13, the measured $_{98}$Cf, $_{99}$Es, and $_{100}$Fm isotope cross sections are compared with calculated populations using Eq. (8) and parameters derived from the experimental light-product isotope distributions as indicated in the figure. The values of $\bar{E}_{tot}$ for Es and Fm are those from Table II; that for $_{98}$Cf is read from Fig. 5. The dotted curve in Fig. 13 represents the Fm case where the total excitation energy is shared between

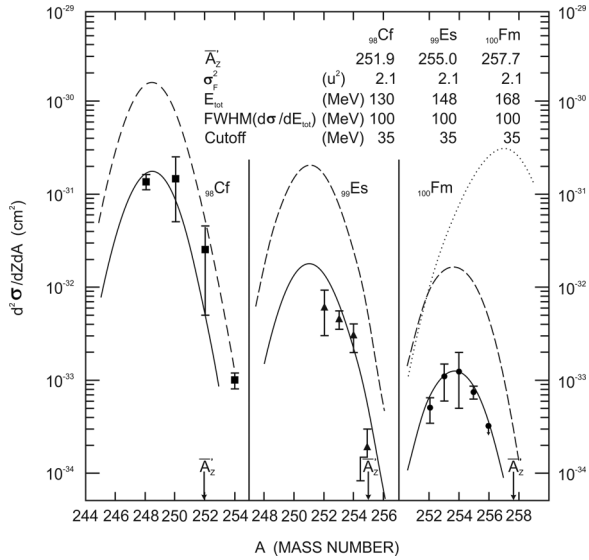

FIG. 13. Comparison of measured (symbols) and calculated isotope populations (curves) for the heaviest actinide elements observed in the ^{238}U + ^{238}U reaction at $\leqslant$7.50 MeV/u. The calculations are outlined in the text. Adapted from Schädel *et al*. [7].

the fragments in proportion to their primary masses. Because isotopes close to $\bar{A}'_Z$ are not observed experimentally and the centroid of the curve is too neutron rich, we conclude first that the energy distributions fall off steeper than with a Gaussian shape at the lowest excitation energies. We take care of this steeper decrease by approximating it by a sharp energy cutoff. An energy cutoff of 35 MeV yields the dashed curves in Fig. 13, which reproduce the position and width of the experimental distributions, but still fail to reproduce the absolute cross sections by one order of magnitude. This discrepancy may be explained by (i) shell effects, (ii) lower Γ_n/Γ_f values as compared to the empirical systematics [45] owing to angular momentum effects, or (iii) nonstatistical processes leading to nonequilibrium states in the exit channel. Assuming (i) may be correlated with the simultaneous formation of a nearly magic, spherical light fragment with $Z = 82$ or $N = 126$, which does not take up much excitation energy and leads, hence, to an increased depletion by fission of the heavy fragments. Agreement between experiment and our estimates is indeed obtained (see solid curves in Fig. 13) if, starting with $Z_h = 98$, it is assumed that the total excitation energy in the low-energy collisions is concentrated in the heavy fragment. Independent of shell closures, a general tendency for the acceptors of mass and charge in damped collisions to carry the total excitation energy and for the donors to stay cold was observed by Klein and Wirtz *et al*. [46,47] in the ^{51}V + ^{197}Au damped collisions. This could be a general handicap for the attempt to produce heavy elements in ^{238}U + ^{238}U or ^{248}Cm collisions. As for (ii), based on the rotating liquid drop model, Γ_n/Γ_f can be expressed [48] as

$$\left(\frac{\Gamma_n}{\Gamma_f}\right)_l = \left(\frac{\Gamma_n}{\Gamma_f}\right)_{l=0} \cdot \exp -\left(\frac{l^2}{l^2_{\rm lim}}\right), \qquad (9)$$

where $l_{\rm lim}$ is a limiting angular momentum which is a function of the temperature of the nucleus and its moment of inertia in the ground state and at the saddle point. Assuming an evaporation cascade with $n = 4$ and fragment spins given by Ref. [13], one obtains again a reduction of the cross sections by about one order of magnitude. As for (iii), the theoretical approach is valid only if the fragments in the exit channel are fully equilibrated. However, it has been shown [8] that for very heavy fragments in the ^{238}U + ^{238}U reaction such an assumption might not be valid. Fragment deformations to shapes more elongated than the respective saddle-point shapes might be associated with large charge transfers.

e. Excitation functions for surviving actinides in $^{238}U + ^{238}U$ collisions. As we have seen in Sec. III A 4 c, the excitation functions of surviving actinides behave similarly with an increase in cross section up to about 6.8 MeV/u and a more flat decrease beyond. Such a shape can be reproduced with the idea of a constant excitation energy bin being responsible for the production of surviving actinides. The solid line in Fig. 12 shows the predicted $_{98}$Cf cross sections from a calculation consistent with the previously made assumptions: (i) the excitation energies of ^{98}Cf fragments can be deduced from the excitation energies of the complementary light fragments, (ii) the Q-value dispersion has a width of 100 MeV (FWHM) [5,6], (iii) there is an energy cutoff of 35 MeV [7], and (iv) the production of the surviving $_{98}$Cf products is governed by the 4n channel. Their survival probabilities were again calculated based on the empirical systematics [45]. The absolute values again disagree with the experimental ones by about an order of magnitude and the same reasons discussed in Sec. III A 4 d are likely to account for this discrepancy.

B. The ^{238}U + ^{248}Cm reaction

1. Actinide cross sections in the $^{238}U + ^{248}Cm$ reaction

The formation cross sections for transcurium isotopes in the ^{238}U + ^{248}Cm reaction at $\leqslant$7.40 MeV/u [44] are shown in Fig. 14. They are compared with thick-target cross sections for the ^{238}U + ^{238}U reaction at 7.50 MeV/u incident energy. The independence of the cross sections of the survivors of the primary heavy actinide isotopes from the projectile energies discussed in Sec. III A 4 b for the ^{238}U + ^{238}U reaction tells us that the cross sections for $_{98}$Cf, $_{99}$Es, and $_{100}$Fm are three to four orders of magnitude higher than in the ^{238}U + ^{238}U reaction owing to the reduced number of protons to be transferred from the target. For ^{259}No, we measured an upper cross section limit of 30 nb.

The measured cross sections for the much less fissile projectilelike fragments $_{84}$Po and $_{85}$ At are about the same in the ^{238}U + ^{248}Cm reaction and in the ^{238}U + ^{238}U reaction indicating that the integral, primary actinide yield distribution is nearly the same in both reactions. This suggests that also the primary actinide yields before fission are about the same for a given (ΔZ, ΔN) transfer in both systems.

2. Comparison of the actinide cross sections in ^{238}U collisions ($\leqslant$7.50 MeV/u) with ^{238}U and ^{248}Cm ($\leqslant$7.40 MeV/u)

The experimental observation of largely different cross sections for the surviving evaporation residues of targetlike

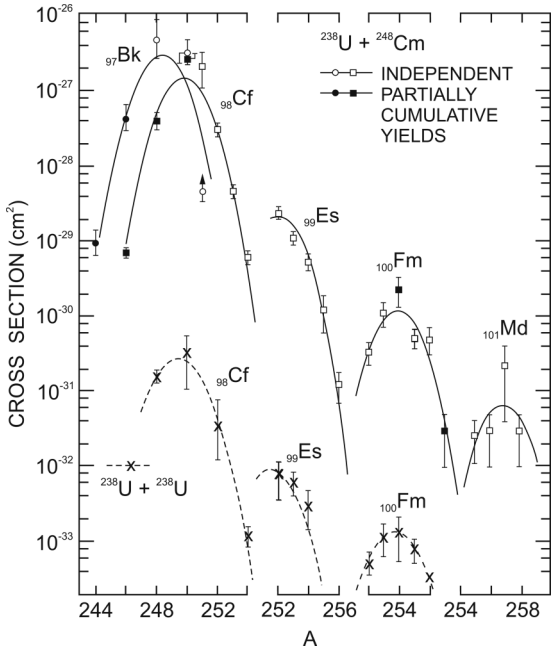

FIG. 14. Cross sections for the formation of targetlike transcurium isotopes in the ^{238}U + ^{248}Cm reaction at $\leqslant$7.40 MeV/u. For comparison, the data for the ^{238}U + ^{238}U reaction at $\leqslant$7.50 MeV/u are also shown. The curves are drawn to guide the eye. The lower limit for the yield of ^{251}Bk is based on γ-ray intensities of $\leqslant$70% at 177 keV and $\leqslant$30% at 153 keV. Adapted from Schädel *et al.* [44].

fragments from the same (ΔZ, ΔN) channels could either indicate differences in the reaction mechanism (which is unlikely) or simply reflect the different survival probabilities of the then different product nuclei. To test the latter hypothesis, we assume that for the same (ΔZ, ΔN) channels, excitation energies and angular momenta are the same. Then it is reasonable to approximate the ratios of cross sections σ(U + U)/σ(U + Cm) for a given channel by the ratio of relative neutron decay widths

$$\prod_{i=1}^{x} \langle \Gamma_n / \Gamma_{\rm tot} \rangle_{i({\rm U+U})} \Big/ \prod_{i=1}^{x} \langle \Gamma_n / \Gamma_{\rm tot} \rangle_{i({\rm U+Cm})}, \qquad (10)$$

using angular-momentum independent, effective values of Γ_n/Γ_f averaged over x deexcitation steps, such as the empirical values of Sikkeland *et al.* [45]. Inherent in this approach is the assumption that modifications of the fission probabilities by excitation energy and angular momentum cancel to a good approximation. Starting from the measured yields for $_{95}$Am ($\Delta Z = 3$) through $_{97}$Bk ($\Delta Z = 5$) in the ^{238}U + ^{238}U reaction [7], [40], we calculated cross sections for $_{99}$Es ($\Delta Z = 3$) through $_{101}$Md ($\Delta Z = 5$) in the ^{238}U + ^{248}Cm reaction [44] for given values of x. The results (Fig. 15) show that an average of $x = 3$ to 4 evaporated neutrons is consistent with the data for the heavier actinides implying average excitation energies of about 30 to 40 MeV in the surviving heavy fragments. This is also consistent with the difference between the observed mass numbers $\bar{A}_Z$ and the primary mass numbers calculated by minimization of the potential energy [27–29] for two touching nuclei, where $\bar{A}'_Z - \bar{A} = x$. The

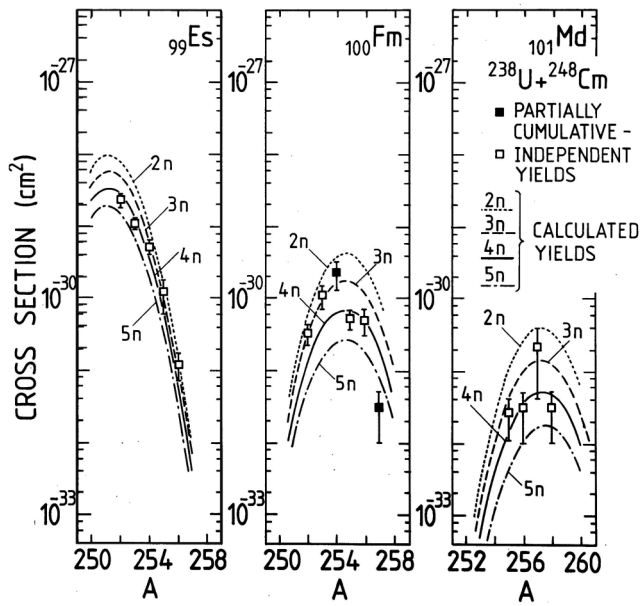

FIG. 15. Comparison of the measured (symbols) and calculated (curves) for the isotope populations in the ^{238}U + ^{248}Cm reaction. The calculations for the 2*n*-5*n* reactions are outlined in the text. Adapted from Schädel *et al.* [44].

values of $x = 3$ to 4 are consistent with our conclusions arrived at in Sec. III A4d. where, however, additional assumptions were required to arrive at the absolute cross sections. The virtue of the present analysis is that it is free from such additional assumptions.

IV. COMPARISON OF THE ELEMENT YIELDS IN THE ^{238}U + ^{238}U/^{248}Cm COLLISIONS WITH DIFFUSION-MODEL PREDICTIONS

In the theoretical work by Riedel and Nörenberg [13], the phenomenological model [10–12,14] for the analysis of dissipative heavy-ion collisions has been extended to treat also cases where thick targets are used. In the interval between the maximum incident energy $E_{\rm m}$ and the Coulomb barrier $V_{\rm C}$, the loss of energy of the ^{238}U beam in the thick target is proportional to the distance from the target surface. Therefore, the energy-averaged element distribution is given by

$$\frac{d\bar{\sigma}}{dZ} = \frac{1}{E_m - V_C} \int_{V_C}^{E_m} dE \frac{d\sigma(E)}{dZ}. \qquad (11)$$

In the phenomenological model, the element distribution for a given sharp incident energy E is determined by

$$\frac{d\sigma(E)}{dZ} = \frac{2\pi}{k^2} \int_0^{l_{gr}(E)} dl \cdot l \cdot P(Z, \tau(l)), \qquad (12)$$

with the solution

$$P(Z, \tau(l)) = [4\pi D_Z \tau(l)]^{-1/2} \cdot \exp\{-(Z - Z_p)^2 / 4 D_Z \tau(l)\} \qquad (13)$$

of a Fokker-Planck equation for a constant diffusion coefficient D_Z and zero drift velocity. $\tau(l)$ is the interaction time as a function of incident angular momentum l. The analysis

of various heavy-ion collisions has taught that for a given projectile-target combination, the interaction time is a function of the impact variable $x = l/l_{gr}$ for different incident energies. Therefore, the approximation

$$\tau(E, l) \equiv \tau(l/l_{gr}) = \tau(x) \tag{14}$$

is used for interaction times corresponding to different incident energies in a thick target. Using an average diffusion coefficient D_Z for the energy interval $[V_C, E_m]$, one obtains according to Eq. (11) for the element distribution in a thick-target experiment

$$\frac{d\bar{\sigma}}{dZ} = \frac{1}{E_m - V_C}\int_{V_C}^{E_m} \sigma_R(E)dE \cdot \int_0^1 p(x)P(Z, \tau(x))dx = \bar{\sigma}_R p_1(Z). \tag{15}$$

Here, the notion $\sigma_R(E) = \pi l_{gr}^2(E)/k^2$ for the reaction cross section as a function of E and $p(x) = 2x$ for the probability distribution of the impact variable x $(0 \leqslant x \leqslant 1)$ have been introduced. Because of the energy averaging in a thick-target experiment, the probability distributions of various quantities are considerably different from those for a thin target with a sharp incident energy. These have been worked out in detail in Ref. [13].

In Fig. 16, the calculated element distribution [Eq. (15)] with an average diffusion coefficient $D_Z = 0.9 \times 10^{22}$ s^{-1} is compared with the experimental data of this work at 7.50 MeV/u incident energy. The theoretical results for $p_1(Z)$ have been normalized to the experimental reaction cross section of ≈1 b. Deviations from the experimental points close to the target charge $Z = 92$ are attributable to the upper limit unity in the second integral in Eq. (15). This

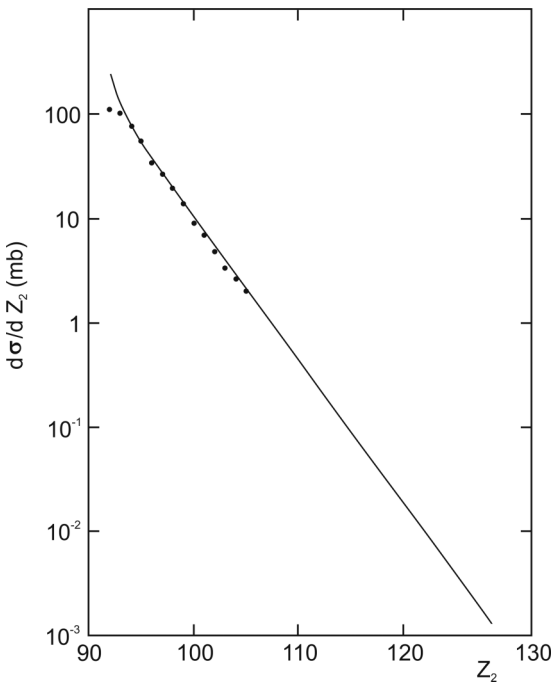

FIG. 16. Element distribution for ^{238}U + ^{238}U at ⩽7.50 MeV/u in a fit of the diffusion coefficient to the experimental data. Adapted from Riedel *et al.* [13].

was not adjusted to improve the agreement in this region of Z. The excellent reproduction of the experimental element yields more distant from the symmetric charge gave some confidence for the extrapolation of the theoretical calculations into the region of heavier fragments. Probabilities of, e.g., $p(E^*, Z)$ were calculated up into the region of $Z = 120$, which are three orders of magnitude smaller as compared to $Z = 100$. Compared to the energy thresholds of about 35 MeV associated with the production of heavy actinides determined in this work, the theoretical thresholds are systematically too low; e.g., a threshold of 35 MeV is associated with production of $Z = 116$ and not with $Z = 98$–100, which is required by the experimental data. Therefore, we have made no attempt to reproduce the experimental $_{98}$Cf, $_{99}$Es, and $_{100}$Fm data on the basis of the theoretical probabilities $p(E^*,Z)$. Rather, we have compared the integral element yields below $Z = 92$ with the theoretical predictions which, in this region, should be less dependent on low-energy thresholds. Figure 7 indicates that there is agreement of the theoretical predictions with the experimental cross sections at 7.65–8.30 MeV/u and at 6.06–7.50 MeV/u. At 6.06–6.49 MeV/u, i.e., in the energy bin closest to the Coulomb barrier, there is a marked disagreement between the experimental element yields and the diffusion-model prediction with the former being a factor of about 5 lower than theory. This is associated with the choice of a constant impact variable $x = l/l_{gr} = 0.7$ at all incident energies which results in a constant ratio of cross sections $\mathrm{DIR}_{prim}/\sigma_r = 0.51$ independent of bombarding energy. Experimentally, this is clearly not the case as we have shown in Sec. III A3 that the ratios $\mathrm{DIR}_{prim}/\sigma_r$ for ^{238}U + ^{238}U collisions are 0.20 in the energy bin 6.06–6.49 MeV/u, 0.38 at ⩽7.50 MeV/u, and 0.55 in the energy bin 7.65–8.30 MeV/u; i.e., they depend markedly on the incident energy. As we have stated in Sec. III A3, large reductions of mass and charge diffusion at near-barrier energies were also reported in Refs. [28,38,39].

In the much more recent theoretical work by Zagrebaev and Greiner [1–4], mass transfer is treated in a Langevin-type equation for the mass asymmetry η,

$$\frac{d\eta}{dt} = \frac{2}{A_{CN}} D_A^{(1)}(\eta) + \frac{2}{A_{CN}}\sqrt{D_A^{(2)}(\eta)}\Gamma(t), \tag{16}$$

which has been derived from the corresponding master equation for the distribution function. Here $\Gamma(t)$ is the normalized random variable with Gaussian distribution, $\langle\Gamma(t)\Gamma(t')\rangle = 2\delta(t - t')$ and $D_A^{(1)}$ and $D_A^{(2)}$ are the transport coefficients. A is the number of nucleons in one of the fragments and the mass asymmetry $\eta = (2A - A_{CN})/A_{CN}$. Assuming that sequential nucleon transfers $A' = A \pm 1$ occur, leads to

$$D_A^{(1)} = \lambda(A \to A + 1) - \lambda(A \to A - 1),$$
$$D_A^{(2)} = \tfrac{1}{2}[\lambda(A \to A + 1)] + \lambda(A \to A - 1)].$$

For nuclei, the macroscopic transition probability $\lambda(A \to A \pm 1)$ is replaced by the nuclear level density

$$\lambda^{(\pm)} = \lambda_0\sqrt{\rho(A \pm 1)/\rho(A)}.$$

The shell correction in the level density parameter is damped in the usual way with increasing excitation energy. λ_0 is the

nucleon transfer rate ($\approx 10^{22}$ s^{-1}). A linear dependence of the diffusion coefficient on nuclear temperature is assumed. The double differential cross sections are calculated as

$$\frac{d^2\sigma_\eta}{d\Omega dE}(E,\Theta) = \int_0^\infty bdb \frac{\Delta N_\eta(b,E,\Theta)}{N_{\rm tot}(b)} \frac{1}{\sin(\Theta)\Delta\Theta\Delta E}, \tag{17}$$

where $\Delta N_\eta(b, E, \Theta)$ is the number of events at a given impact parameter b in which the system enters into the channel η with kinetic energy E and outgoing angle Θ in the center of mass; $N_{\rm tot}(b)$ is the total number of simulated events. Equation (17) describes the mass, energy, and angular distributions of the *primary* fragments formed in the binary reaction. Subsequent deexcitation cascades via fission and emission of light particles and γ rays are taken into account for each event. The sharing of the excitation energy between the primary fragments is assumed to be proportional to their masses.

In Fig. 17, the evaporation residue cross sections for the production of heavy nuclei in damped collisions of ^{238}U with ^{248}Cm at 800 MeV center-of-mass energy (not for 7.40 MeV/u ^{238}U incident on a thick target) are shown along with the data of this work. As can be seen, many more neutron-rich isotopes of superheavy elements are predicted to be produced: New isotopes of elements 105 and 106 are shown by the open circles.

A. Perspectives

The diffusion models by both Riedel and Nörenberg [13] and by Zagrebaev and Greiner [1–4] give little hope to reach superheavy elements close to $Z = 114$ with measurable cross sections in reactions such as ^{238}U + ^{248}Cm. However, Fig. 17 suggests that a search for hitherto undiscovered neutron-rich isotopes in the region of elements 105 through 108 with cross sections >1 pb [3,4] might be attractive. For longer-lived isotopes of elements 104, 105, and 106 this might even be possible with chemical separations as the chemical properties of these elements are well known [49]. For short-lived isotopes, magnetic separators such as large-aperture solenoids are under discussion and might eventually open the way to many interesting new isotopes.

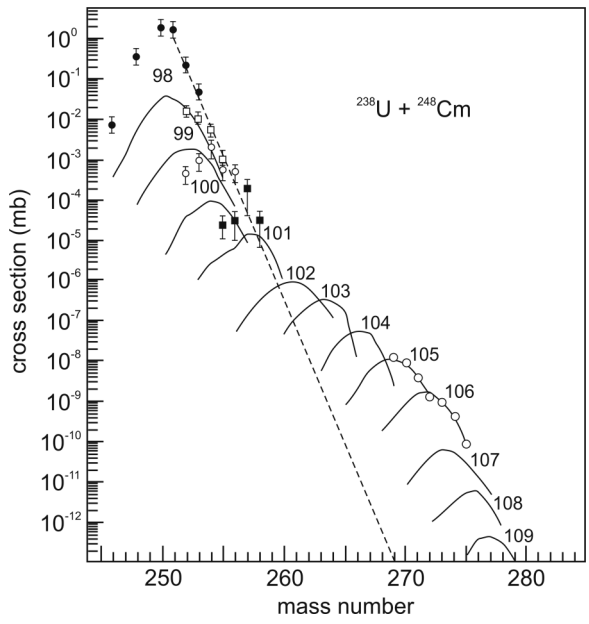

FIG. 17. Cross sections of surviving isotopes of superheavy elements produced in collisions of ^{238}U with ^{248}Cm at 800 MeV center-of-mass energy. Experimental data for Cf, Es, Fm, and Md from this work are also shown. The dashed line shows the expected locus of the cross section in the absence of shell effects. From Zagrebaev *et al*. [4].

V. SUMMARY

In the present work, we have reexamined data on mass and charge distributions in collisions of ^{238}U projectiles with thick targets of ^{238}U and ^{248}Cm at near-barrier energies, which showed that fission is an important reaction channel in these collisions. In the ^{238}U + ^{238}U reaction at $\leqslant$7.50 MeV/u, the large number of measured isotope cross sections was used to construct a rather complete surface of independent yields in the *Z-A* plane that was decomposed into partial cross sections for surviving products from quasielastic collisions, deep-inelastic collisions, and for the associated sequential fission processes. The reconstructed primary distributions for these reaction channels have cross sections relative to the total reaction cross section $\mathrm{QER}_{\rm prim}/\sigma_r = 0.62$ and $\mathrm{DIR}_{\rm prim}/\sigma_r = 0.38$. The experimental centroids $\bar{A}_Z$ of the Gaussian isotope distributions for elements $79 \leqslant Z \leqslant 91$ have been used, by comparison with calculated centroids $\bar{A}'_Z$ derived by minimization of the potential energy for two touching liquid drops with corrections for neutron-pair breaking δn, to estimate the average number of neutrons $\bar{\nu}_Z$ evaporated from the primary fragments and to deduce from this the associated average excitation energies $\bar{E}_Z$. These were used to calculate total excitation energies $\bar{E}_{\rm tot}$ and the average values of $\overline{\rm TKEL}$ as a function of Z. These were compared with values of $\overline{\rm TKEL}$ determined at 7.42 MeV/u in a counterexperiment [5,6] using thin targets. For small charge exchanges, the thick-target values of $\overline{\rm TKEL}$ are typically about 30 MeV smaller than the thin-target values with the difference decreasing with increasing charge exchange developing into even slightly larger values in the thick-target experiment for the largest charge transfers. This corresponds to the expected trend. The reconstructed relative cross sections $\mathrm{DIR}_{\rm prim}/\sigma_r$ in the energy bins 6.06–6.49 MeV/u and 7.65–8.30 MeV/u are 0.20 and 0.55, respectively. Thus, these values show a strong energy dependence which is not reproduced by the phenomenological diffusion model by Riedel and Nörenberg [13] with the choice of a constant impact variable $x = l/l_{\rm gr} = 0.7$.

Cross sections for surviving heavy actinides in the ^{238}U + ^{238}U reaction are an order of magnitude larger than in the reaction ^{136}Xe + ^{238}U, showing, consistently with the relatively low values of $\overline{\rm TKEL}$ as a function of Z, that more particle diffusion occurs in the ^{238}U + ^{238}U reaction than in other collision systems at a given dissipated energy. Heavy actinide cross sections in the ^{238}U + ^{238}U reaction were measured at $\leqslant$7.50 MeV/u and in other bins of incident energies. We have shown that these cross sections are associated with the low-energy tails of the dissipated energy

distributions, however, with an empirical low-energy cutoff on the order of 35 MeV. With this cutoff and an empirical set of $\Gamma_n/(\Gamma_n + \Gamma_f)$ values, we have been able to reproduce the shape and position of the isotope distributions of the surviving actinides and their bombarding energy dependence but have failed to reproduce the absolute cross sections by one order of magnitude. Additional assumptions that could remove this problem have been discussed. In a comparison of the survival probabilities of targetlike heavy actinides for the same $(\Delta Z, \Delta N)$ transfers in the $^{238}\mathrm{U} + ^{238}\mathrm{U}$ and $^{238}\mathrm{U} + ^{248}\mathrm{Cm}$ reactions, the absolute cross sections could be reproduced for the $3n$ and/or $4n$ evaporation channels without the need for additional assumptions. *A posteriori*, this corroborates the low-energy cutoff of 35 MeV. Theoretical predictions of evaporation-residue cross sections with a Langevin-type equation and subsequent statistical-model evaporation/fission calculations in the $^{238}\mathrm{U} + ^{248}\mathrm{Cm}$ reaction seem to indicate that the production of superheavy elements close to $Z = 114$ with measurable cross sections is unrealistic, but there are more realistic prospects for the production of new neutron rich isotopes of elements 105 through 108 that might warrant experimental efforts.

[1] V. I. Zagrebaev, Yu. Ts. Oganessian, M. G. Itkis, and W. Greiner, Phys. Rev. C **73**, 031602(R) (2006).
[2] V. Zagrebaev and W. Greiner, J. Phys. G: Nucl. Part. Phys. **34**, 2265 (2007).
[3] V. Zagrebaev and W. Greiner, Nucl. Phys. A **787**, 363c (2007).
[4] V. Zagrebaev and W. Greiner, Phys. Rev. C **78**, 034610 (2008).
[5] K. D. Hildenbrand, H. Freiesleben, F. Pühlhofer, W. F. W. Schneider, R. Bock, D. von Harrach, and H. J. Specht, Phys. Rev. Lett. **39**, 1065 (1977).
[6] H. Freiesleben, K. D. Hildenbrand, F. Pühlhofer, W. F. W. Schneider, R. Bock, D. von Harrach, and H. J. Specht, Z. Phys. A **292**, 171 (1979).
[7] M. Schädel, J. V. Kratz, H. Ahrens, W. Brüchle, G. Franz, H. Gäggeler, I. Warnecke, G. Wirth, G. Herrmann, N. Trautmann, and M. Weis, Phys. Rev. Lett. **41**, 469 (1978).
[8] P. Glässel, D. von Harrach, Y. Civelecoglu, R. Männer, H. J. Specht, J. B. Wilhelmy, H. Freiesleben, and K. D. Hildenbrand, Phys. Rev. Lett. **43**, 1483 (1979).
[9] C. Lebrun, F. Hanappe, J. F. Lecolley, F. Lefèbres, C. Ngô, J. Pétèr, and B. Tamain, Nucl. Phys. A **321**, 207 (1979).
[10] G. Wolschin and W. Nörenberg, Z. Phys. A **284**, 209 (1978).
[11] S. Ayik, G. Wolschin, and W. Nörenberg, Z. Phys. A **286**, 71 (1978).
[12] C. Riedel, G. Wolschin, and W. Nörenberg, Z. Physik A **290**, 47 (1979).
[13] C. Riedel and W. Nörenberg, Z. Physik A **290**, 385 (1979); C. Riedel (private communication).
[14] R. Schmidt and G. Wolschin, Z. Physik A **296**, 215 (1980).
[15] S. Grossmann, Z. Physik A **296**, 251 (1980).
[16] H. Gäggeler, N. Trautmann, W. Brüchle, G. Herrmann, J. V. Kratz, P. Peuser, M. Schädel, G. Tittel, G. Wirth, H. Ahrens, H. Folger, G. Franz, K. Sümmerer, and M. Zendel, Phys. Rev. Lett. **45**, 1824 (1980).
[17] J. V. Kratz, W. Brüchle, H. Folger, H. Gäggeler, M. Schädel, K. Sümmerer, G. Wirth, N. Greulich, G. Herrmann, U. Hickmann, P. Peuser, N. Trautmann, E. K. Hulet, R.W. Lougheed, J. M. Nitschke, R. L. Ferguson, and R. L. Hahn, Phys. Rev. C **33**, 504 (1986).
[18] H. Folger and U. Richter, Nucl. Instrum. Methods **167**, 85 (1979).
[19] M. Schädel, W. Brüchle, B. Haefner, J. V. Kratz, W. Schorstein, N. Trautmann, and G. Herrmann, Radiochim. Acta **25**, 111 (1978).
[20] L. C. Nothcliffe and R. I. Schilling, Nucl. Data Tables A **7**, 233 (1970).
[21] W. Brüchle, H. Folger, and J. V. Kratz, GSI Scientific Report 1979, GSI (1980), p. 121.
[22] R. W. Lougheed, E. K. Hulet, R. L. Landingham, M. Nitschke, H. Folger, J. V. Kratz, W. Brüchle, and H. Gäggeler, Nucl. Instrum. Methods **200**, 71 (1982).
[23] J. V. Kratz, J. O. Liljenzin, and G. T. Seaborg, Inorg. Nucl. Chem. Lett. **10**, 951 (1974).
[24] N. Hildebrand, C. Frink, N. Greulich, U. Hickmann, J. V. Kratz, N. Trautmann, G. Herrmann, M. Brügger, H. Gäggeler, K. Sümmerer, and G. Wirth, Nucl. Instrum. Methods A **260**, 407 (1987).
[25] R. Gunnink and J. B. Niday, Report UCRL-51061 (1971).
[26] U. Reus, W. Westmeier, and I. Warnecke, Report GSI 79-2 (1979).
[27] V. V. Volkov, in *Proceedings of the International Conference on Reactions between Complex Nuclei, Nashville 1974* (North-Holland, Amsterdam, 1974), Vol. II, p. 363.
[28] J. V. Kratz, W. Brüchle, G. Franz, M. Schädel, I. Warnecke, G. Wirth, and M. Weis, Nucl. Phys. A **332**, 477 (1979).
[29] H. Freiesleben and J. V. Kratz, Phys. Rep. **106**, 1 (1984).
[30] J. V. Kratz, J. O. Liljenzin, A. E. Norris, and G.T. Seaborg, Phys. Rev. C **13**, 2347 (1976).
[31] U. Reus, A. M. Habbestad-Wätzig, R. A. Esterlund, P. Patzelt, and I. S. Grant, Phys. Rev. Lett. **39**, 171 (1977).
[32] J. V. Kratz, A. E. Norris, and G. T. Seaborg, Phys. Rev. Lett. **33**, 502 (1974).
[33] R. J. Otto, M. M. Fowler, D. Lee, and G. T. Seaborg, Phys. Rev. Lett. **36**, 135 (1976).
[34] J. Poitou, J. V. Kratz, G. Wirth, and R. Lucas, Nucl. Instrum. Methods **180**, 221 (1981).
[35] J. V. Kratz, J. Poitou, W. Brüchle, H. Gäggeler, M. Schädel, G. Wirth, and R. Lucas, Nucl. Phys. A **357**, 437 (1981).
[36] W. Reisdorf, Modified version of the code ALICE (private communication).
[37] K. Wolfsberg, Report LA-5553-MS (1974).
[38] H. Essel, K. Hartel, W. Henning, P. Kienle, H. J. Körner, K. E. Rehm, P. Sperr, W. Wagner, and H. Spieler, Z. Physik A **289**, 265 (1979).
[39] K. E. Rehm, H. Essel, P. Sperr, K. Hartel, P. Kienle, H. J. Körner, R. E. Segel, and W. Wagner, Nucl. Phys. A **366**, 477 (1981).
[40] M. Schädel, Doctoral dissertation, University of Mainz, 1979; GSI-Report 79-8 (1979).
[41] H. J. Becker, T. Lund, R. Brandt, D. Molzahn, and H. Jungclas, GSI Scientific Report 1977, GSI (1978), p. 74.
[42] K. L. Wolf, J. P. Unik, E. P. Horwitz, C. A. A. Bloomquist, and W. Delphin, Bull. Am. Phys. Soc. **22**, 67 (1977); K. L. Wolf (private communication).
[43] M. Dakowski, P. Doll, A. Gobbi, G. Rudolf, H. Sann, R. Bock, U. Lynen, and A. Olmi, Phys. Lett. B **90**, 379 (1980).

[44] M. Schädel, W. Brüchle, H. Gäggeler, J. V. Kratz, K. Sümmerer, G. Wirth, G. Herrmann, R. Stakemann, G. Tittel, N. Trautmann, J. M. Nitschke, E. K. Hulet, R. W. Lougheed, R. L. Hahn, and R. L. Ferguson, Phys. Rev. Lett. **48**, 852 (1982).

[45] T. Sikkeland, A. Ghiorso, and M. J. Nurmia, Phys. Rev. **172**, 1232 (1968).

[46] P. Klein, J. V. Kratz, M. K. Gober, H. P. Zimmermann, W. Brüchle, W. Reisdorf, and M. Schädel, Z. Phys. A **357**, 193 (1997)

[47] Ch. Wirtz, J. V. Kratz, W. Brüchle, M. Schädel, B. Schausten, and N. Wiehl, Radiochim. Acta **89**, 689 (2001).

[48] K. H. Schmidt, W. Faust, G. Münzenberg, W. Reisdorf, H. G. Clerc, D. Vermeulen, and G. Lang, *Proceedings of the International Conference on Physics and Chemistry of Fission, Jülich 1979*, IAEA- SM/241-C8 (1979).

[49] J. V. Kratz, in *Handbook of Nuclear Chemistry*, edited by A. Vértes, S. Nagy, Z. Klencsár, R. G. Lovas, and F. Rösch (Springer Science + Business Media, Berlin, 2011), Vol. 2, Chap. 20, pp. 926–1004.